High velocity sand erosion

MSc Thesis

Oliver O.A. Heijmeijer
April, 2019

TU Delft Delft University of Technology

Boskalis

High velocity sand erosion

MSc Thesis

Author:
Oliver O.A. Heijmeijer

Graduation committee

Prof. dr. ir. C. van Rhee	**Delft University of Technology**
Dr. Ir. G.H. Keetels	**Delft University of Technology**
Dr. Ir. A.J. Nobel	**Royal Boskalis Westminster**
Dr. Ir. M van Damme	**Delft University of Technology**

TU Delft Delft University of Technology

Boskalis

Preface

In the figure below one can see the progress made by an average master student during their thesis. First, one has to learn what they don't know. Then, when they know what they don't know, they have to become good at the latter. As shown in the graph, this goes faster as time passes.

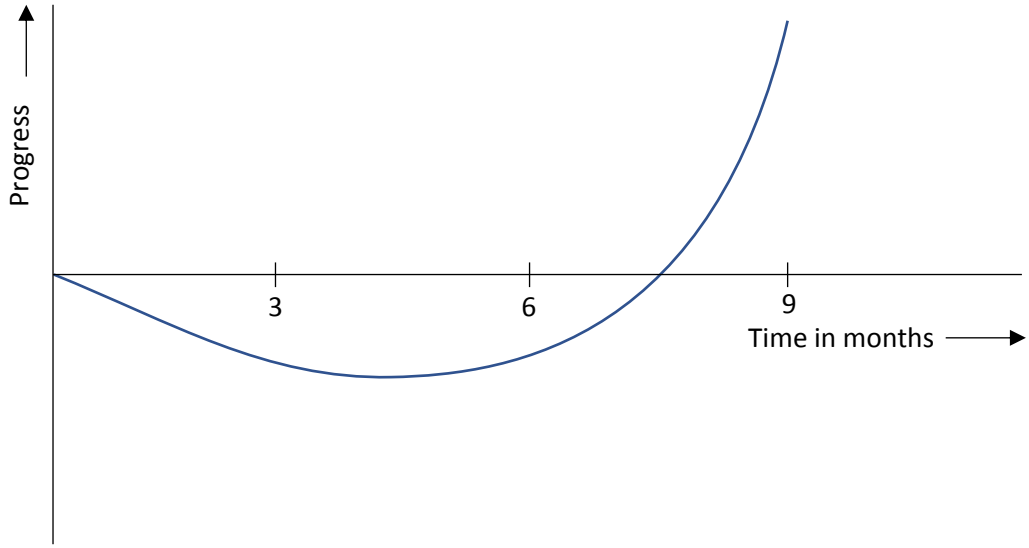

It has not been an easy ride. But it has been fantastically reassuring to always receive help and support from the people around me. To my parents, brother and sister, fellow students and friends: thanks for all the chats and advice! To Arno, Cees and Geert, my supervisors and prof: thank you for guiding me along the path from not knowing what I didn't know, to being a MSc!

Oliver Heijmeijer
Rotterdam, March 2019

Summary

Understanding the erosion process of sand will help improve dredging projects. Pickup functions are used to predict the amount of sand that can be eroded by a flow with certain parameters. The most common functions that are used have been validated to data in the low velocity regime ($\theta < 1$). However, modern day dredging processes are in the high velocity erosion regime ($\theta > 1$).
An example of such a function is the widely used pickup function of Van Rijn (1984). It predicts the pickup of grains well at low flow velocities, but overestimates pickup at high flow velocities.
Recently Bisschop (2018) has performed erosion experiments at high flow velocities. BOKA (2015) also performed experiments in the same velocity regime during a preliminary study. However, a different setup was used. It was found that there is a large (factor 2) discrepancy between the two studies.

The present study has performed experiments with a setup similar to that of Van Rijn (1984), however, the flow velocity was not limited to the low velocity regime. Erosion tests were done with bed shear stresses up to 60 Pa ($\theta<30$). The setup in question uses a sediment lift to push a prepared sand bed up into the flow.
The determination of the bed shear stress was questionable in preliminary study of BOKA (2015). Since it is a very important parameter in erosion predictions, it was a focus of the present study to determine the bed shear stress accurately. The bed shear stress was determined with three different methods which all agree within an acceptable range (up to 8%).
The erosion velocity is determined by measuring the lift velocity, which is equal to the erosion velocity when the top of the sand bed is level with the floor of the setup. Whether the top of the sand bed is level or not has been determined with the use of a high speed camera.
In the table below one can see the parameters of the experiments carried out by the present study.

Parameter	u_{flow} [m/s]	τ_b [Pa]	θ [-]	d_{50} [µm]	n_0 [-]	ρ_s [kg/m^3]
Value	1 - 4.7	23802	0.5 - 30	125	43 - 47	2650

Table 1: Parameters of experiments

The produced data has been compared to existing data and pickup functions of other studies. In Figure 1 the comparison can be seen. It is clear that no existing functions match the data of the present study.

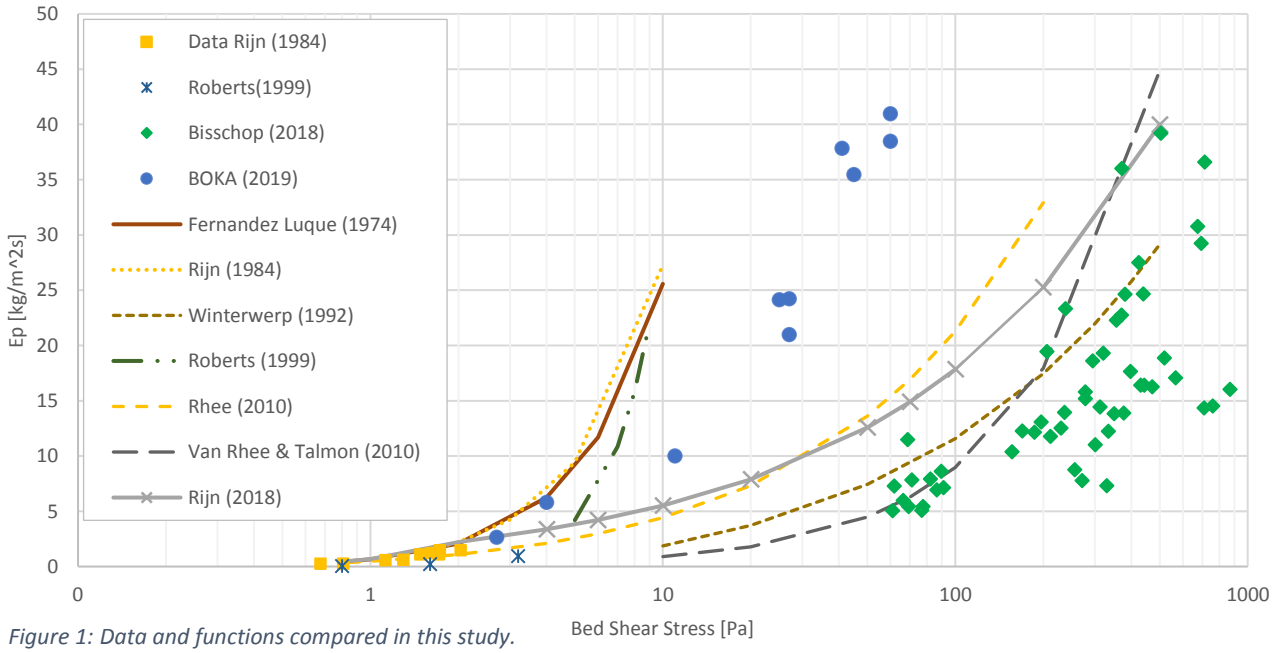

Figure 1: Data and functions compared in this study.

During the experiments of the different studies, the bed shear stress has either been measured over a fixed sand bed (τ_f) or over a mobile sand bed (τ_m). The functions that overestimate the data of BOKA (2019) correspond to τ_f and all the functions that underestimate the data of BOKA (2019) correspond to τ_m. The function of Van Rhee (2010) is the only exception since it has been validated to both types of experiments. Because τ_m is not yet fully understood, τ_f has been used in the newly presented function (Equation (4.5)).
In the overestimating functions the critical shields parameter maintains a strong influence on the pickup as the flow velocity increases. It is argued that the critical shields parameter is a low velocity parameter and must therefore become less important as the flow velocity increases. The newly presented function adjusts the use of the critical shields parameter accordingly.

Figure 2 presents the new function compared to the data of Bisschop (2018) and the present study. The pickup values of Bisschop (2018) have been coupled to the corresponding values of τ_f for the comparison. It can be seen that the newly presented function matches the data of BOKA quite well. Also, one can see that the function can predict erosion at higher values of the near bed concentration when one assumes a fixed bed for the determination of the bed shear stress.

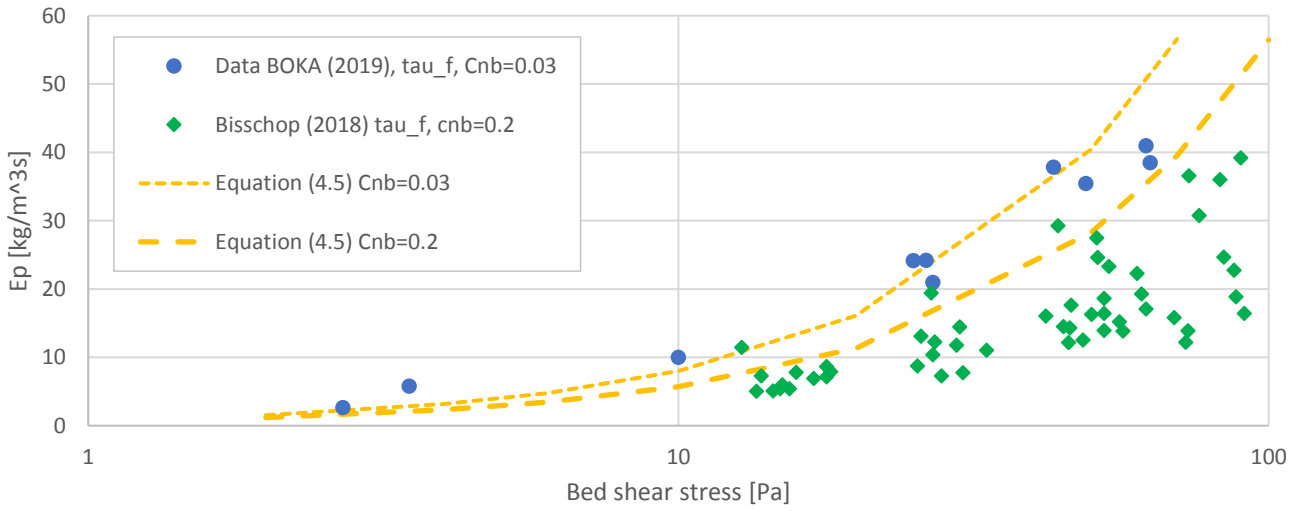

Figure 2: New function presented by the present study compared to the data of the present study and the data of Bisschop (2018)

Contents

List of symbols

Roman Letters

A	Cross sectional area	$[m^2]$
A_b	Bed associated area	$[m^2]$
A_w	Wall associated area	$[m^2]$
C	Chézy coefficient	$[\sqrt{m}/s]$
C_d	Drag coefficient	[-]
C_k	Cozeny - Karman coefficient	[-]
C_L	Lift coefficient	[-]
c	Concentration	[-]
c_b	bed concentration	[-]
c_{nb}	Near bed concentration	[-]
D_h	Hydraulic diameter	[m]
$D_{h,b}$	Bed associated hydraulic diameter	[m]
$D_{h,w}$	Wall associated hydraulic diameter	[m]
D_*	Dimensionles grain diameter	[-]
d	diameter	[m]
d_{10}	Diamter at which 10% of the grains is smaller	[µm]
d_{30}	Diamter at which 30% of the grains is smaller	[µm]
d_{50}	Diamter at which 50% of the grains is smaller	[µm]
d_{60}	Diamter at which 60% of the grains is smaller	[µm]
d_{90}	Diamter at which 90% of the grains is smaller	[µm]
dp	Differential pressure	[Pa]
dp_b	Differential pressure over the bed assosiated area	[Pa]
dp_w	Differential pressure over the wall associated area	[Pa]
E	Nett erosion flux	$[kg/m_2s]$
E_p	Pickup flux	$[kg/m_2s]$
E_{ph}	Hindered Pikcup flux	$[kg/m_2s]$
F_d	Drag force	[N]
F_L	Lift force	[N]
g	Acceleration of gravity	$[m/s^2]$
h	height	[m]
i	hydraulic gradient	[-]
k	Permeability	[m/s]
k_l	Permeability at maximum porosity	[m/s]
k_r	Roughness height	[m]
L	Length	[m]
n	Emprical constant Richardson and Zaki	[-]
n_0	Porosity	[-]
n_l	maximum porosity	[-]
Re	Reynolds number	[-]
Re_b	Bed associatd Reynolds number	[-]
Re_p	Particle Reynolds number	[-]
$Re_{p,w}$	Particle Reynolds number used for settling velocity	[-]
S	Settling Flux	$[kg/m_2s]$
T	Transportation term	[-]
u_{flow}	Depth averadged flow velocity	[m/s]
Vm	Volume of mixture	$[m^3]$
v_e	Erosion velocity	[mm/s]
w_s	Settling velocity	[m/s]

Greek Letters

ß	Angle of sand bed	[rad]
Δ	Relative grain density	[-]
δ	Damping factor	[-]
ϕ	Internal friction angle	[-]
κ	Von Karman constant	[-]
λ	Roughness factor	[-]
ν	Kinematic viscosity	[m^2/s]
ρ	Density	[kg/m^3]
ρ_s	Grain density	[kg/m^3]
ρ_w	Water density	[kg/m^3]
τ	Shear stress	[Pa]
τ_b	Bed shear stress	[Pa]
τ_f	Bed shear stress over a fixed bed	[Pa]
τ_m	Bed shear stress over a mobile bed	[Pa]
τ_w	Wall shear stress	[P]
θ_b	Shields parameter	[-]
θ'	Adapted Shields parameter	[-]
θ_{cr}	Critical Shields parameter	[-]
θ'_{cr}	Adapted critical Sields parameter	[-]

1. Introduction

1.1. Background

Dredging activities are very important in our modern society. Examples of such activities are maintenance of coastlines, ports and rivers, building of new ports and islands and digging trenches for pipelines or cables. These activities al have in common that soil needs to be relocated. Before the soil can be transported, it is loosened and brought into suspension so that it can be pumped as a mixture. This often happens by means of water jets. Water jets in the industry typically produce flow velocities up to 50 m/s. Loosening the soil and bringing it in suspension is called erosion. Understanding the erosion processes will help improve dredging processes.

Erosion takes place naturally in rivers or at coastlines, for example, due to the flow of the water. In these locations flows are in the order of 1 m/s. For this process there are several functions to predict the amount of erosion corresponding to a certain flow. The Pickup Function of Van Rijn (1984) is commonly used.

The bed shear stress (τ_b) is a more representative parameter for the erosion process than the flow velocity. Henceforth, this parameter will be used in stead of the flow velocity to compare data. A dimensionless shear stress called the Shields parameter (θ) is also used. Commonly, erosion due to a flow with $\theta>1$ is referred to as high-velocity erosion. Both parameters will be explained in detail in Chapter 2.

As mentioned above the flow velocities reached during dredging processes are high, therefore, the erosion during dredging is called high-velocity erosion. The functions used to predict the erosion rate have been found to be incorrect at higher flow velocities. Van Rhee (2010) presents a correction term for the function of Van Rijn that includes the influence of the bed properties. The corrected function is validated to data produced during the study of, among others, Roberts (1998). The experiments of Roberts (1998) have been done with shear stresses ranging from 0.2 Pa to 6.5 Pa which corresponds to $0.1 < \theta > 3.2$.

During the current study, erosion experiments have been done at high flow velocities (up to 4.7 m/s) with bed shear stresses up to 60 Pa ($\theta = 30$). The produced data has been compared to existing functions and a new function is presented which is based on the data of the present study as well as the existing functions.

1.2. Problem definition

- The existing pickup function of Van Rijn (1984) matches experimental data quite well in the low-velocity region ($\theta < 1$), however, it largely overestimates the erosion velocity at higher flow velocities. The recent study of Bisschop (2018) has produced data with flow velocities up to 6 m/s corresponding, in that setup, to shear stress values up to 900 Pa ($\theta = 445$). Although the erosion during these experiments is clearly high velocity erosion, the data shows a discrepancy with the corrected pickup function of Van Rhee (2010).
- The erosion process is complex and depends on many variables (e.g. velocity of the flow, concentration above the bed or particle size). The relation between erosion velocity and these variables in existing studies is not yet thoroughly understood.
- In addition to the above-mentioned problems, there is a clear discrepancy (Figure 1.1, more than a factor 2 in erosion velocity) between the data of Bisschop (2018) and data gathered by Boskalis in 2015 during a preliminary set of experiments. Because the experimental setups of both studies and the flow velocities are very similar, one would expect the results to be closer together.

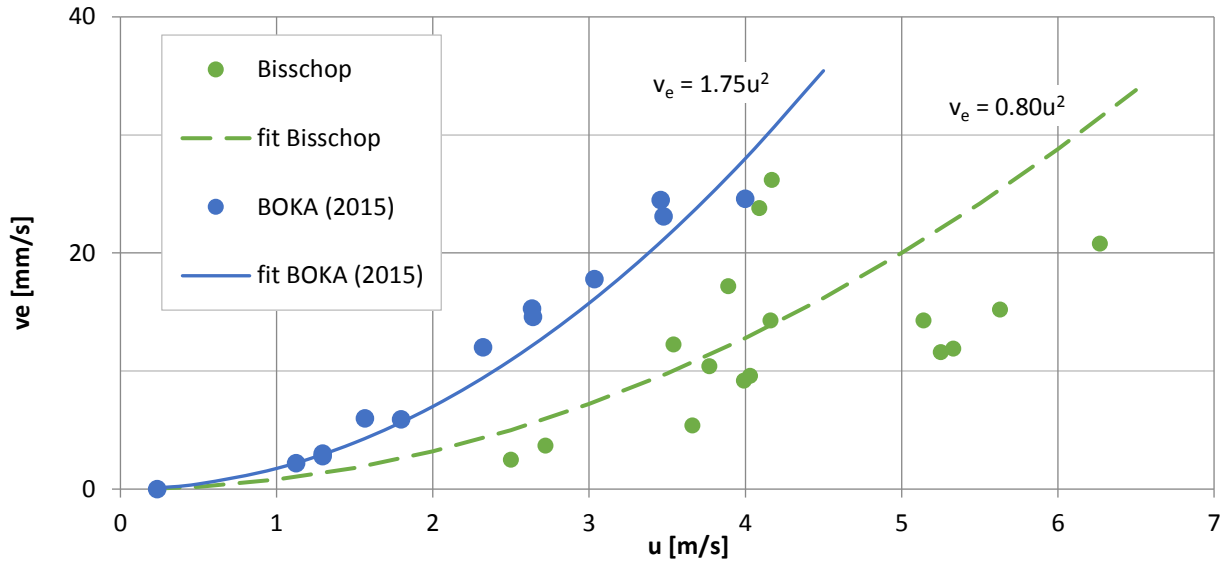

Figure 1.1: Initial comparison of erosion velocities.

1.3. Research objective

- Produce a reliable dataset in addition to that of Bisschop (2018) in a test setup like that of Van Rijn (1984) and Roberts (1998).
- Compare the data produced during the study with the data of Bisschop (2018) and provide an explanation for the difference.
- Validate the pickup functions of Fernandez Luque (1974), Van Rijn (1984), Winterwerp (1992), Roberts (1998), the correction of Van Rhee (2010) and Cheng (2016).

2. Theory

The supporting theory for this research is explained in this chapter, starting with the general erosion process. The paragraph includes the stability criterium of a grain and several existing pickup functions. Additionally, one of the most important parameters of this study, shear stress, is addressed.

2.1. General process

2.1.1. Erosion velocity

Erosion of a sand bed is governed by the amount of sand that is picked up by the flow and the amount of sand that settles. These amounts are expressed as fluxes: the pickup flux E_p and the settling flux S [kg/m^{2}s]. The net erosion flux E is the actual amount of sand that is removed and transported from the bed (Equation (2.1)).

$$E = E_p - S \tag{2.1}$$

where $E_p \geq 0$ and $S \geq 0$. The surface of a sand bed can be seen as an interface between the water and the sand bed itself. In a situation where $E_p < S$, the interface will move up (sedimentation) and when $E_p > S$ the interface will move down (erosion) (Figure 2.1). The velocity at which the interface moves down is called the erosion velocity (v_e) and, following from the mass balance, is defined as:

$$v_e = \frac{E_p - S}{\rho_s(1 - n_0 - c_{nb})} \tag{2.2}$$

in which:

ρ_s:	Density of sand grain	[kg/m^3]
c_{nb}:	Near bed concentration	[-]
n_0:	In situ porosity	[-]

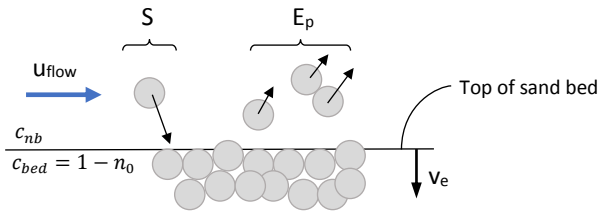

Figure 2.1: Eroding sand bed

2.1.2. Settling velocity

The settling flux is defined by:

$$S = \rho_s w_0 c_{nb}(1 - c_{nb})^n \tag{2.3}$$

where w_0 is the settling velocity of a single grain and n is calculated with the method of Rowe (1987):

$$n = \frac{4.7 + 0.41\, Re_{p,w}^{0.75}}{1 + 0.175\, Re_{p,w}^{0.75}} \tag{2.4}$$

Richardson & Zaki (1954) provide a function for the settling velocity of a grain in a mixture with a concentration c (w_s). In such an environment the grains settle more slowly due to the effect called hindered settling.

$$w_s = w_0(1 - c)^n \tag{2.5}$$

w_0 is the settling velocity of a single grain in a stationary water column and is described by the well-known equation for the settling velocity of a sphere:

$$w_0 = \sqrt{\frac{4\Delta g d}{3C_D}} \tag{2.6}$$

in which:

g: Gravitational acceleration	[m/s^2]
d: Diameter of sphere	[m]
Δ: $(\rho_s - \rho_w)/\rho_w$ (specific density)	[-]
ρ_s: Sand grain density	[kg/m^3]
ρ_w: Water density	[kg/m^3]
C_D: Drag coefficient	[-]

The C_D is the drag coefficient and is a function of the particle Reynolds number. There are three relations between the C_D and particle Reynolds number depending on the flow regime:

Particle Reynolds nr. $$Re_{p,w} = \frac{w_0 \cdot d}{\nu} \tag{2.7}$$

Laminar regime $$Re_{p,w} < 1 : C_D = \frac{24}{Re_{p,w}}$$

Transition regime $$1 < Re_{p,w} < 2000 : C_D = \frac{24}{Re_{p,w}} + \frac{3}{\sqrt{Re_{p,w}}} + 0.34 \tag{2.8}$$

Turbulent regime $$Re_{p,w} > 2000 : C_D = 0.4$$

To determine the C_D in the transition regime, iteration is necessary. However, one can choose to use the explicit approximation of the settling velocity of Ferguson and Church (2004):

$$w_0 = \frac{\Delta g d^2}{\alpha_1 \nu^2 + \sqrt{0.75 \alpha_2 \Delta g d^3}} \tag{2.9}$$

In which:

$\alpha_1 = 18$

$\alpha_2 = 1$ for natural sands and 0.44 for spheres

ν: kinematic viscosity [m^2/s]

In reality one should account for the fact that sediments consist of multiple fractions of grain diameters. The present study focusses on a sediment with a very narrow particle size distribution, however, so the effect of multiple fractions will not be taken into account. For a narrow grain size distribution one can use the mean diameter of the grain (d_{50}) in the calculation of the settling velocity.

2.1.3. Stability of a grain

The forces that act on a grain are lift (F_L), drag (F_D), shear (F_s), friction (F_ϕ) and the submerged weight (F_w) (Figure 2.2). The friction force F_ϕ is a combination of all the contact forces with other grains and the actual friction along the surface of the grain. This force is a function of the submerged weight of the grain and the angle of the sand bed at which grains start moving due to gravity (Equation (2.11)). In the figure one can also see the point M, about which the grain can rotate. The first three forces are caused by the fluid flowing over the grain and are therefore referred to as the fluid forces (F_{fluid}). These forces are the driving forces that contribute to moving the grain and are expressed as:

$$\left.\begin{aligned} F_L &= u^2\rho_w \cdot A_L c_L \\ F_D &= u^2\rho_w \cdot A_D c_D \\ F_S &= u^2\rho_w \cdot A_S c_S \end{aligned}\right\} \quad F_{fluid} \propto u^2\rho_w d^2 \tag{2.10}$$

where A_L, A_D and A_S are the corresponding surfaces which are all a function of d^2. c_L, c_D, c_S are constants that depend mainly on the shape of the object in the flow. u is the height averaged flow velocity.

The last two forces mentioned above are referred to as the resisting forces (F_{res}) since they contribute to keeping the grain in place. These forces are expressed as:

$$\left.\begin{aligned} F_w &= (\rho_s - \rho_w) \cdot g \cdot \frac{\pi}{6} d^3 \\ F_\phi &= F_w \cdot \tan\phi \end{aligned}\right\} \quad F_{res} \propto (\rho_s - \rho_w) g d^3 \tag{2.11}$$

Where g is the gravitational acceleration and ϕ is the internal friction angle of the sand.

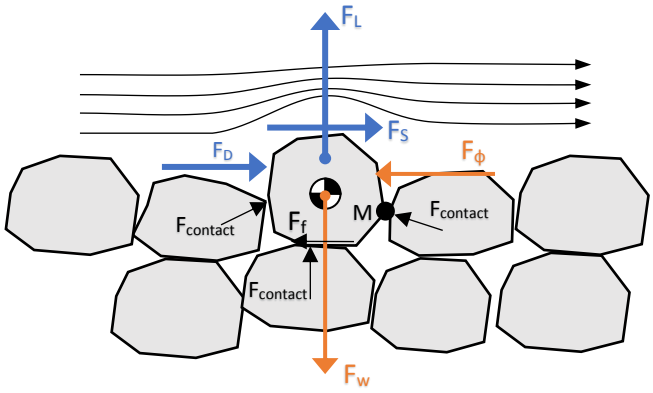

Figure 2.2: Forces on a grain in a sand bed and streamlines over sand bed

The stability of the grain depends on the balance between the driving fluid forces and the resisting forces. When the lift force and submerged weight counteract each other and the drag, shear and friction force counteract each other, the grain is in balance. When the fluid forces overcome the resistance forces however, the grain will start to move. This balance can be described by the following proportional relationship:

$$u^2\rho_w d^2 \propto (\rho_s - \rho_w) g d^3 \tag{2.12}$$

By adding an unspecified parameter c to Equation (2.12) it may be written as:

$$u^2\rho_w d^2 = (\rho_s - \rho_w) g d^3 \cdot c \tag{2.13}$$

Rewriting Equation (2.13) gives:

$$c = \frac{u^2}{\Delta g d} \tag{2.14}$$

This leads to the well-known Shields parameter θ which is a non-dimensional shear stress, is in the same form as Equation (2.14) and is defined as:

$$\theta = \frac{u_*^2}{\Delta g d} = \frac{\tau_b}{(\rho_s - \rho_w) g d} \tag{2.15}$$

With the Darcy-Weisbach friction factor λ and the shear velocity u_*, the bed shear stress τ_b is defined by:

$$\tau_b = \frac{\lambda}{8} \rho_w u^2 = u_*^2 \rho_w \tag{2.16}$$

The Darcy-Weisbach friction factor can be estimated with the Colebrook (1939) Equation.

$$\frac{1}{\sqrt{\lambda}} = -2 \log\left(\frac{k_r}{3.7 D_h} + \frac{2.51}{Re \cdot \sqrt{\lambda}}\right) \tag{2.17}$$

where k_r is the roughness height of the bed. With the cross sectional area A and the perimeter P of a pipe, D_h is the hydraulic diameter and is defined as:

$$D_h = \frac{4A}{P} \tag{2.18}$$

R_e is the Reynolds number and is defined as:

$$Re = \frac{u \cdot D_h}{\nu} \tag{2.19}$$

2.1.4. Critical shields number

The moment when a grain loses its stability and starts moving is called the critical moment. Therefore, the shields number corresponding to that moment is called the critical shields number. There are numerous functions to determine the critical shields number, however a widely used function is that of Brownlie (1981):

$$\theta_{cr} = 0.22 Re_p^{-0.6} + 0.06 \exp\left(-17.77 Re_p^{-0.6}\right) \tag{2.20}$$

Where the particle Reynolds number is defined as (different than Equation (2.7)):

$$Re_p = \frac{d\sqrt{\Delta g d}}{\nu} \tag{2.21}$$

In a study of Miedema (2010) it is shown that the critical shields value depends on the exposure of a grain to the flow. When a grain is more exposed it will be easier to pick up than when it is flush with the grains around it. However, for the current study this effect is not taken into account since the exposure of the grains will be randomly distributed over the bed including strongly exposed and less exposed grains.

2.1.5. Existing pickup models

Over the years, many studies have been done to figure out the complicated process of erosion. In this paragraph the models that where significant to this study are explained. All models are a combination of several principle terms and take the form of:

$$\Phi_p = \frac{E_p}{\rho_s \sqrt{\Delta g d_{50}}} = n \cdot T^m \tag{2.22}$$

Where ϕ_p is the dimensionless pickup flux, n and m are empirical constants and T is the transport parameter. In the table below one can find an overview of the different pickup functions.

Source	n	T	m	
Fernandez Luque (1974)*	0.02	$\theta - \theta_{cr}$	1.5	(2.23)
Van Rijn (1984)	$0.00033 \cdot D_*^{0.3}$	$\frac{\theta - \theta_{cr}}{\theta_{cr}}$	1.5	(2.24)
Winterwerp (1992)	$0.012 \cdot D_*^{0.3}$	$\theta^{0.5} - 1.3$	1	(2.25)
Roberts (1998)				(2.26)
Van Rhee (2010)**	$0.00033 \cdot D_*^{0.3}$	$\frac{\theta - \theta'_{cr}}{\theta'_{cr}}$	1.5	(2.27)
Van Rhee & Talmon (2010)	$0.0025 \cdot (D_* - 2.4)^{0.3}$	θ	1	(2.28)
Cheng (2016)	$0.0001 \cdot D_*^{2.5}$	$F_* \exp\left(-\frac{40}{F_*}\right)$	1	(2.29)
Van Rijn (2018)***	$0.00033 \cdot D_*^{0.3} \cdot \frac{1}{\theta}$	$\frac{\theta - \theta_{cr}}{\theta_{cr}}$	1.5	(2.30)

Table 2.1: Overview of the different pickup functions regarded in this study

* : *The value of n is proposed by Van Rijn (1984).*

** : *See Equation (2.34) for* θ'_{cr}

*** : *This function is only valid for* $\theta > 1$. *For* $\theta < 1$ *Equation (2.24) is used*

where D_* is the dimensionless particle diameter :

$$D_* = d_{50} \sqrt[3]{\frac{\Delta g}{\nu^2}} \tag{2.31}$$

and F_* is the densiometric Froude number:

$$F_* = \frac{u}{\sqrt{\Delta g d_{50}}} \tag{2.32}$$

Equation (2.32) has a direct relation with the shields parameter: $F_* \propto \sqrt{\theta}$

In Table 2.2 one can see an overview of the parameters of the experiments carried out by the different studies mentioned in the table above. Since Van Rhee (2010) and Van Rijn (2018) did not do experiments, but validated theoretical analyses to data of other studies, they are not shown in Table 2.2.

Source	uflow [m/s]	θ [-]	d50 [µm]	n0 [-]	cnb [%]	Flume type	Bed length [cm]	Location on bed
Fernandez Luque (1974)	-	-	900 - 3300*	-	-	2	500 - 700	-
Van Rijn (1984)	0.5 - 1	0.3 - 1	130 - 1500	0.4	0	1	2 - 5	1
Winterwerp (1992)	-	0.6 - 8.2	134 - 225	-	0 - 45**	3	1500 - 900	2
Roberts (1998)	-	0.1 - 3.2	5 - 1350	0.4 - 0.6	0	1	15	1
Van Rhee & Talmon (2010)	-	0 - 22	125 - 185	-	0 - 30	2	630	2
Cheng (2016)	0.27 - 0.99	0.01-0.54	230 - 860	0.4 -0.44	0	1	1.5	1
Bisschop (2018)	1.5 - 6	2.5 - 450	51-562	0.4 - 0.5	~ 0.25	2	630	2
BOKA (2019)	1 - 4.7	2.9 - 32	125	0.43 - 0.47	0	1	20	1

Table 2.2: Parameters of experiments done by studies considered during the present study.

** : Density of the grains was also varied during these experiments.*
*** : Depth averaged concentration*

where the different flume types are:
1. Sand bed with lift
2. Sand bed without lift
3. Sand bed under an angle

and the different locations on the bed where the erosion velocity has been measured are:
1. Over the entire bed (for short beds). The bed shear stress is measured over a fixed bed (τ_f)
2. At a significant distance downstream of the start of the bed. Here there will be a developed concentration profile. The bed shear stress is measured over the mobile bed (τ_m).

2.1.6. Dilatancy reduced erosion

Van Rhee (2010) found that the pickup function of Van Rijn (1984) largely overestimates the pickup at high flow velocities. Van Rhee (2010) proposes to include the effect of dilatancy by adding a correction factor to the critical shields number.

In Figure 2.3 one can see a close-up of a sand bed where the top layer has been sheared to the right. As the figure shows, the pore volume has increased after shearing. The increase in volume is called dilatancy. The new space will be filled by the water surrounding the sand bed. The hydraulic gradient caused by the inflow of water will resist the dilation of the layers of sand. Van Rhee (2010) states that the porosity of the sand bed must change from the in-situ porosity n_0 to the maximum porosity n_l before it can be eroded. The maximum porosity is a characteristic of the sediment and can be determined from geotechnical tests. By combining Darcy's law for hydraulic gradient and the necessary increase in porosity, Van Rhee (2010) gives the following equation for the hydraulic gradient:

$$i = -\frac{v_e}{k_l} \cdot \frac{n_l - n_0}{1 - n_l} \tag{2.33}$$

where k_l is the permeability of the soil at the maximum porosity n_l. This equation is only valid in the top layer of the sand bed. By combining the traditional critical shields number (Equation (2.20)) and Equation (2.33), Van Rhee (2010) defines a corrected shields parameter:

$$\theta'_{cr} = \theta\left(\frac{\sin(\phi-\beta)}{\sin\phi} + \frac{v_e}{k_l}\cdot\frac{n_l-n_0}{1-n_l}\cdot\frac{A}{\Delta}\right) \tag{2.34}$$

in which $A = 3/4$ for single grains and $A = \frac{1}{1-n_0} \approx 1.7$ for a continuum. The left term inside the brackets of Equation (2.34) includes the loss of shear strength of a bed under an angle ß. For the current study however, only horizontal beds are considered, therefore, the term is not explained. Because the value of ß is 0 for a horizontal bed, the discussed term becomes 1.
Van Rhee (2010) gives a criterion for high velocity erosion, i.e. the moment when Equation (2.34) should be used: When the right term between the brackets (Equation (2.34)) becomes of order unity. Since all the values in this term, except v_e, are characteristics of the soil and are constant, Van Rhee (2010) defines the criterium for high velocity erosion as:

$$\frac{v_e}{k_l} > \frac{n_l-n_0}{1-n_l}\cdot\frac{A}{\Delta} \tag{2.35}$$

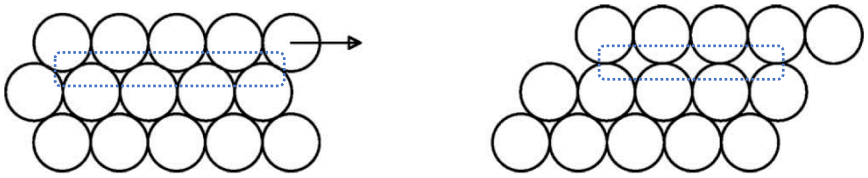

Figure 2.3: Increase of pore volume due to shear of an arrangement of particles (Van Rhee, 2010)

2.1.7. Hindered erosion

During erosion, the pickup flux is influenced by the near bed concentration (c_{nb}). Bisschop (2018) calls this influence hindered erosion. If the near bed concentration is high, there will be a lot of grain-grain interaction where grains will be knocked back onto the bed. Additionally, turbulence, which is a driver for pickup (Cao, 1997), is suppressed by a high (c_{nb}).
Another effect is described by Van Rhee & Talmon (2010) which continues on the theory that pickup is determined by turbulent bursts. They introduce a reduction factor (Equation (2.36)) that takes a down-flow into account. Since an eddy is circular, it has an up-flow on one side and a downflow on the other side (Figure 2.4). The up-flow causes grains to be picked up from the bed to the flow. The theoretical maximum amount of grains that can be picked up is the concentration of the sand bed: $1-n_0$. At the same time, the eddy transports other grains from the flow to the bed, due to the downflow. Therefore, the net pickup is reduced. The maximum concentration that can be transported from the flow to the bed is the near bed concentration c_{nb}. The difference in concentration is therefore a factor for the reduction of the net pickup, which, in this study, is referred to as hindered pickup. When the $c_{nb} = 0$ the net pickup is not reduced and when $c_{nb} = 1-n_0$ the net pickup is reduced to 0.

$$E_{ph} = E_p \cdot \left(\frac{1-n_0-c_{nb}}{1-n_0}\right) \tag{2.36}$$

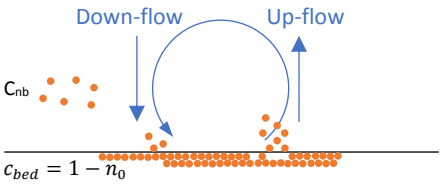

Figure 2.4: A turbulent eddy above the sand bed picks up grains and replaces others at the same time.

2.1.8. Erosion regimes

During erosion, different regimes are recognized: the saltation regime and the bed load (or sheet flow) regime (van Rijn, 1984). The saltation regime describes a relatively slow flow in which the grains are lifted off of the bed individually and transported a certain distance. Single grains are lifted off of the bed due to lift, drag and shear along the bed. In this regime it looks like the grains are jumping, hence the name saltation.

In the sheet flow regime a layer of grains rolls/slides over the sand bed at relatively high flow velocities. Gao (2008) gives a theoretical model describing the transition between the saltation regime and the sheet flow regime as the bed shear stress τ increases (Figure 2.5). At higher values of the bed shear stress, one finds a combination of saltation, rolling and sliding. Sheet flow starts occurring when the bed shear stress overcomes the shear strength of the sand bed, causing whole layers of sand to start sliding.

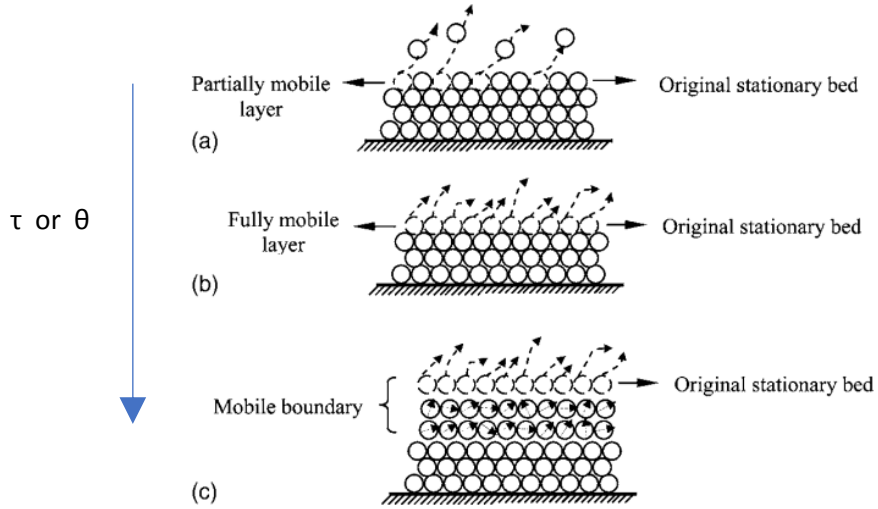

Figure 2.5: Diagram showing bed conditions: a) saltation regime; b) onset of sheet-flow regime; and c) sheet flow-regime (Gao, 2008)

2.2. Shear stress

2.2.1. General wall shear stress

A flow over a bed experiences resistance due to friction with the bed and wall. The velocity of the fluid at the bed and walls is zero. Each 'layer' of fluid closer to the center of the pipe moves slightly faster, but is held back by the layer below it due to viscous shear in the fluid. A laminar flow has this viscous shear throughout the entire height of the flow. The velocity profile is very smooth and follows a parabolic profile (Figure 2.6). A turbulent flow ($Re > 4000$) has a (thin) boundary layer in which the viscosity must be taken into account. However, in the larger part of the flow, called the inviscid outer flow, the viscosity may be neglected. Therefore there is hardly any shear in this area and the velocity profile does not change much in this area. The profile follows a logarithmic profile. At the height where the velocity is at its maximum, the shear stress is 0. The line drawn in Figure 2.6 at this height is therefore called the zero-shear line. The location of this line depends on the roughness of the bed and walls. From this line outwards the shear stress increases linearly to the maximum shear stress which is at the boundaries. The friction with the wall is a function of the wall roughness. As the roughness increases, the friction increases and thus the shear stress increases. In the previous paragraph the equation for bed shear stress τ_b has been given (Equation (2.16)).

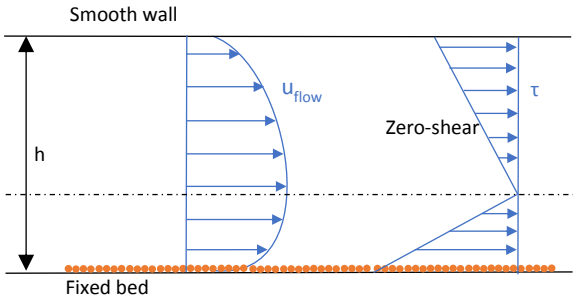

Figure 2.6: 2D representation of Velocity and Shear stress profiles in a pipe with a fixed sand bed

An approach to calculate the wall shear stress (in addition to Equation (2.16)) is using the logarithmic law or law of the wall (Equation (2.37)). Since the wall shear stress is the cause for the shape of the velocity profile, one can use this information to calculate the wall shear stress.

$$\frac{u_z}{u_*} = \frac{1}{\kappa}\ln\left(\frac{z}{z_0}\right) \tag{2.37}$$

In this equation, u_z is the flow velocity at height z, κ is the Von Karman constant (0.4) and z_0 is the height at which the flow velocity is 0. The last parameter can be determined with:

$$z_0 = 0.11\frac{\nu}{u_*} + 0.033k_r \tag{2.38}$$

where k_r is the roughness of the wall in mm.

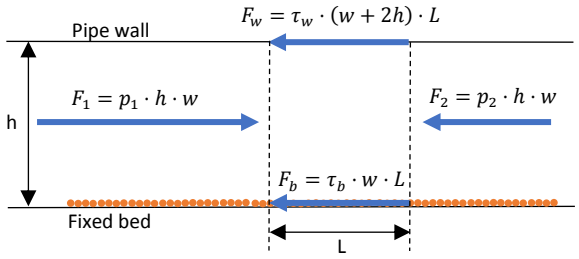

Figure 2.7: Relation between Pressure of flow and shear stress. w is the width of the pipe and h is the height of the pipe

In Figure 2.7 one can see the forces that are present in a square pipe. The arrow in the top of the figure and F_w include the friction force of the vertical walls. The pump produces a pressure (p), which is a force divided by the cross-sectional area. From the figure can be seen that: $F_1 = F_w + F_b + F_2$. Filling in and rewriting this relation gives:

$$dp = \frac{\tau_b wL + \tau_w(w + 2h)L}{wh} \tag{2.39}$$

From Equation (2.39) it can be seen that, when the friction of the walls, and thus the wall shear stress are known, the bed shear stress can be determined by measuring the pressure drop. Pugh & Wilson (1999) give a method to determine the bed shear stress when the wall shear stress is not known. This method is discussed in the next paragraph.

2.2.2. Walls with different roughness

In the case of a pipe where the walls all have the same roughness, the velocity and shear stress profile are symmetrical (about the centerline of the pipe). In the setup of the current study, however, the roughness of the

bottom wall, called the bed, is higher due to the coating of sand (Figure 2.8). This sand is fixed, so it does not erode, but creates a higher roughness. The rough sand bed will experience higher shear stresses than the smooth walls. Pugh & Wilson (1999) present a method with which one can differentiate the different shear stresses of the different walls.
The theory is based on the idea that the flow can be divided into different sections. In the case of the setup of the current study, the flow is divided into a bed associated area A_b and a wall associated area A_w where $A = A_w + A_b$ (Figure 2.8).

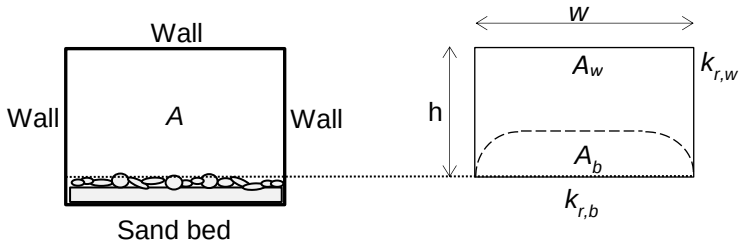

Figure 2.8: Front view of pipe with bed and wall associated areas. The depicted sand grains are magnified for the clarity of the sketch

The line that divides the two areas is the zero-shear line and the pressure drop over a certain length must be the same in both areas:

$$dp_b = \frac{\tau_b \cdot w \cdot l}{A_b} = dp_w = \frac{\tau_w \cdot (2h + w) \cdot l}{A_w} \tag{2.40}$$

where w and h are the width and the height of the pipe respectively, l is the length over which the pressure drop is measured and A_b and A_w are the bed and wall associated areas respectively. When one knows the roughness of the walls and the bed, the corresponding shear stress can be calculated with Equation (2.16) where the hydraulic diameters of the corresponding areas are:

$$D_{h,w} = \frac{4A_w}{2h + w} \qquad D_{h,b} = \frac{4A_b}{w} \tag{2.41}$$

Now the ration A_w/A_b can be adjusted until $dP_b = dP_w$, where A is the total cross-sectional area of the pipe. If one is able to measure the actual pressure drop, the values of the roughness can be adjusted until the measured pressure drop matched dP_b and dP_w.

2.2.3. Shear stress over a mobile bed

As the name suggests bed shear stress is the shear stress related to a sand bed. In this paragraph a distinction is made between shear stress over a fixed bed (τ_f) and a mobile bed (τ_m). In a situation where the sand bed is fixed, the shear stress can be calculated as described in Paragraph (2.2.2).

The friction over a mobile bed is not as straight forward as the friction over a pipe wall with a constant roughness. It is a quite complicated process which is not yet completely understood. Studies have been done though, to achieve a better understanding of the shear stress over a mobile bed. For example, it is shown that when grains are removed from the bed they leave a space behind which increases the roughness and therefore increases the bed shear stress too (Figure 2.5a). In addition to this physical increase in roughness, there are other factors that contribute to an imaginary roughness called effective roughness. The factors that contribute to this effective roughness are:

- Rolling and sliding grains, called a mobile layer (Gao, 2008) (Figure 2.5)
- Acceleration and deceleration of grains leading to a lag velocity (Greimann, 1999).

Whenever there is a pickup flux, the lifted grains will be accelerated by the flow. After some time the grain comes back to the bed and is stopped. This accelerating and stopping is a constant process. On average, one can see that the velocity of the grains is slower than that of the flow. This phenomenon is referred to as lag velocity (Greimann, 1999). The lag velocity can be measured as a pressure loss and can thus be seen as shear stress.

Pugh & Wilson (1999) state that the effective roughness over a mobile bed is a function of the shields parameter:

$$\frac{k_s}{d_{50}} = C \cdot \theta_b \tag{2.42}$$

or

$$\frac{k_s}{d_{50}} = C \cdot \frac{\tau_b}{(\rho_s - \rho_w)g} \tag{2.43}$$

This is an implicit function and iteration is needed to determine the roughness and shear stress, however, the function has more than one solution (Miedema & Matousek, 2014). For this reason, Bisschop (2018) derived his own function and fitted it to the data of his study:

$$\lambda_b = 1.373 \cdot 10^{-9} \cdot Re_b^{1.247} \tag{2.44}$$

where λ_b is the friction factor that can be used in Equation (2.16) and Re_b:

$$Re_b = \frac{u \cdot D_{h,b}}{\nu} \tag{2.45}$$

3. Experiments

3.1. Overview of setup

The setup that has been used in the present study is based on the setup used by Van Rijn (1984) and can be seen in Figure 3.1. Clean water flows from left to right through the horizontal section. The vertical section holds the sand that will be eroded and is pushed upwards by the lift. Roberts (1998) used a similar experimental setup with a relatively low channel height (2 cm).

With the combination of the pump and piping at hand, the maximum (height averaged) flow velocity that can be achieved is 4.7 m/s. The internal width and the height of the setup are respectively 0.188m and 0.113m. The measuring section is 5m from the inflow to make sure that the flow is fully developed once it reaches the sand. The bottom wall of this development section, has been coated with a layer of sand (glued onto wooden boards) to ensure a more realistically developed flow. The sand that has been used to coat the wall is the same as the sand that will be used to erode during the experiments. After passing the measurement section and picking up the sand, the water exits the setup and enters the reservoir. Here, the sand settles and the clean water is reused. Photos of the setup can be seen in Appendix F.

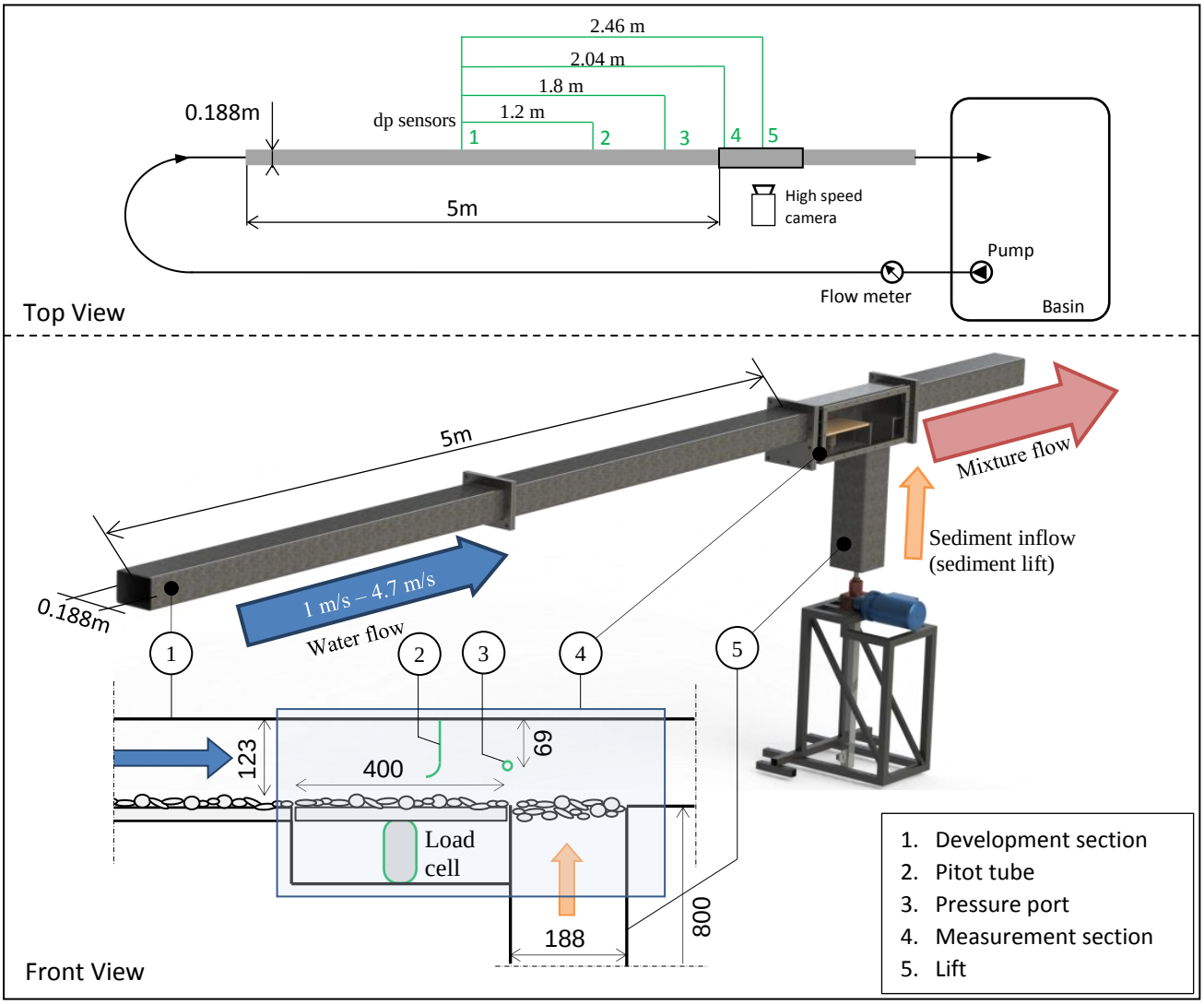

Figure 3.1: Overview of setup. Dimensions in the measurement section are in mm. All sensors are green. The depicted sand grains are magnified for the clarity of the sketch

3.2. Sensors

There are several sensors in this section. The purpose of each sensor is explained below.

- Load cell (in combination with the shear board it measures the bed shear stress)
- Differential pressure sensors (placed at certain distances along the whole setup.
- Pitot tube
- Length sensor for lift
- Flow meter

Load cell

As can be seen in Figure 3.1 the measurement section is higher than the development section. The extra height is needed for a load cell below the so-called shear board. This board is at the same height as the boards in the development section, making a nearly even floor all the way up to the sand bed. The shear board is mounted into the pipe such that it is fixed in y and z-direction, but can move in x-direction. The water flowing over the shear board will apply a force on the board pushing it in the positive x-direction. Since the load cell is mounted to the shear board, it measures the force applied by the water. Dividing this force by the surface area of the board gives the bed shear stress.

Differential pressure sensors

A total of 6 pressure ports have been mounted along the entire length of the pipe. In Figure 3.1 only the last 4 can be seen. The first two are located in the development section in the same wall. Rosemount differential pressure sensors were used to measure the pressure loss between certain points. Using the method of Pugh and Wilson (1999) one can determine a bed shear stress from the measured pressure loss in addition to the measurement of the shear board (Paragraph 2.2.2).

Pitot tube

Pitot tubes have been used to measure the velocity of the flow at different heights, resulting in the velocity profile. One can use the velocity profile and the logarithmic law to calculate the bed shear stress (Paragraph 2.2) This calculation is only valid when the velocity profile has a logarithmic shape.

Position sensor

The position of the lift is measured by the position sensor. One can calculate the velocity of the lift by dividing smalls changes in length by the time that elapsed during the change.

Flow meter

A flow meter in the system measures the flow rate of the water in m^3/h. By dividing the flow rate by the cross-sectional area of the measuring section, one can calculate the depth-averaged velocity at the sand bed.

High speed camera

During the experiments the top of the eroding sand bed was filmed with a high-speed camera. The footage was used to judge if the lift was pushing too fast, at just the right speed, or too slow (Paragraph 3.5). Additionally it was used to inspect the erosion process.

Scale

To measure the weight of the dry sand, a scale was used. The scale had an accuracy of 1gr.

3.3. Properties of sand

During the experiments one type of sand was used. The name of the sand is GEBA, which has a very narrow size distribution (Figure 3.2) and a d_{50} of 125µm. Bisschop (2018) measured the permeability of GEBA at different porosities (Figure 3.3) and used the datapoints to determine the Kozeny-Carman constant (C_k). The permeability can be calculated with the adapted Kozeny-Carman equation of Bear (1972) and Batu (1998):

$$k = C_k \cdot \frac{g}{\nu_w} \cdot d_{10}^2 \cdot \frac{n_i^3}{(1-n_i)^2} \tag{3.1}$$

Grain size				Porosity		Kozeny-Carman
d_{10}	d_{50}	d_{60}	d_{90}	n_{max}	n_{min}	C_k
µm	µm	µm	µm	-	-	-
92	125	133	175	0.506	0.370	0.00387

Table 3.1: Properties of GEBA sand

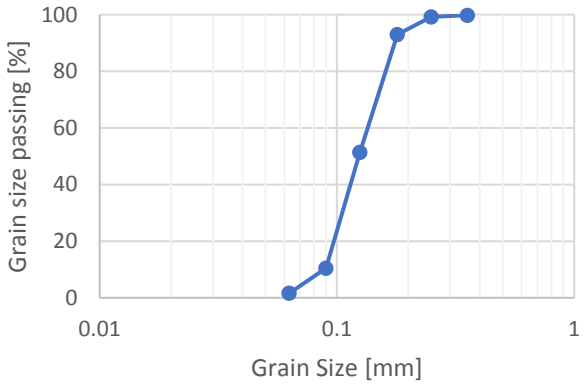

Figure 3.2: Grain size distribution of GEBA

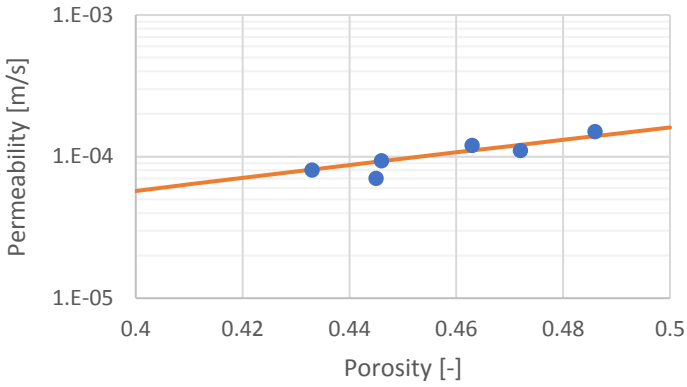

Figure 3.3: Measured and calculated permeability of GEBA sand (Bisschop, 2018)

3.4. Calibration

The 0-value of a sensor is the signal that it transmits when it measures the wanted variable to be zero. During the calibration phase of this study it was noticed that sometimes the measured values had an offset from 0. Most likely external factors, like temperature and humidity, influence the sensors. Therefore, after the sand sample was in place and the setup was filled with water, the flow was brought down to 0m/s. At this velocity all sensors should return the according variable to be 0. If this was not the case, the 0-value of the sensors was adjusted accordingly to remove the offset. In Figure 3.4 one can see that, once corrected, all sensors correctly indicate the corresponding variables to be 0.

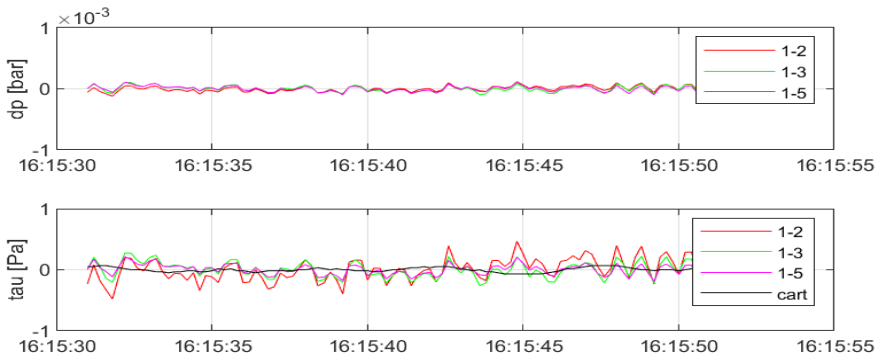

Figure 3.4: Signal of sensors over time at a flow of 0 m/s

3.5. Measuring procedure

First of all the weight of the sand dry sand (moisture content of 0%) was measured. Next the lift shaft was treated with lubricant to ensure that the sand bed and lift seal experienced as little resistance as possible. After that it was filled with water after which the sand was added with care. It is important that no air remains in the sand since this will negatively influence the measurement of the porosity. Since the sand was added after the water and since it was done with care, the grains had time to settle. Therefore, the resulting sand bed was very loose (i.e. high porosity). To reduce the porosity to the desired value the sand bed was shaken by means of a vibrator that was pressed into the sand bed. Once the desired porosity was achieved ($n_0 \approx 0.43$), the sand bed was covered with geotextile and pebbles to ensure that it remained in place while the flow was brought up to speed. Next, the window of the setup was closed and the setup was filled with water. After all the air was cleared by letting the pump run for a short period, the flow was brought to a stop. This was done to be able to set the correct 0-value of the sensors (Paragraph 3.4). After that, the camera was started and the flow was brought to the desired velocity. Next, the lift was started at a preset speed. Depending on the flow velocity, between 1 and 3 lift speeds could be tested before the sand was completely eroded. When all the sand had been eroded, the lift was turned off . Finally the flow was brought to a stop and the setup was emptied.
After running the test, the set lift speeds were qualified to be too slow, equal to v_e or too fast. This was done visually with the aid of the footage of the high speed camera (Figure 3.5). The goal was to have all three qualifications per flow velocity to be able to determine the upper and lower limit of v_e.

a)

b)

c)

Figure 3.5: Qualification of erosion velocity. a) lift speed too slow, b) lift speed = ve, c) lift speed too fast

3.6. Reliability of experiments

The main variables that are of interest during this study are the bed shear stress, the flow velocity, the erosion velocity and the porosity (relative density) of the sand bed. The reliability of the measurement of shear stress, erosion velocity and porosity is discussed below. The reliability and accuracy of the measurement of flow velocity directly depend on the accuracy of the equipment mentioned above.

3.6.1. Bed shear stress

Because the shear stress is an important parameter, the setup of the current study has the option to measure the shear stress in different ways as explained in Paragraph 3.2. In a study of Nobel (2017) and the preliminary study of BOKA (2015) the differential pressure measurements turned out not to be reliable, however. Therefore it was a focus of the current study to make sure the produced data was reliable. At the time the bed shear stress could be measured with the loadcell and with the differential pressure measurements. To increase the reliability of the measurements a pitot tube was added to the setup to be able to measure the velocity profile. As described in Paragraph (2.2.1) one can use the velocity profile to calculate the bed shear stress. With the three different measurements the determined shear stress could be cross-checked.
The method of Pugh & Wilson (1999) is used to calculate the bed shear stress from the measured differential pressures. In Appendix D the process of iteration is shown for the calculation of the bed shear stress using the Pugh & Wilson (1999) method. In this paragraph a brief overview of the different methods is given.

In the next section of the paragraph many symbols will be used that are similar. For that reason the description of the different symbols has been presented in Table 3.2.

Symbol	Description
dp_b or dp_b	Differential pressure belonging to the bed associated area A_b
dp_w or dp_w	Differential pressure belonging to the wall associated area A_w
$\tau_{dp,b}$	Bed shear stress calculated from differential pressure
τ_{lc}	Bed shear stress measured with the load cell
τ_{vp}	Bed shear stress calculated from the velocity profile

Table 3.2: Description of some symbols are presented here for clarity and easy reading.

It is common to use a roughness height that is proportional to a representative grain diameter for a granular bed. The heights range from 1 to 5 times $d_{10}, d_{30}, d_{50}, d_{70}, d_{90}$ (Garcia, 2007). By tweaking the roughness values in the calculation for shear stress, the three measured values for bed shear stress ($\tau_{dp,b}$, τ_{lc} and τ_{vp}) will converge. After several iterations the ratio between wall and bed associated areas (Paragraph 2.2.2) converged to $\frac{A_b}{A} \approx 0.366$. A bed-roughness height of $k_{r,b} = 2 \cdot d_{90} = 350\ \mu m$ and a wall-roughness height of $k_{r,w} = 5\ \mu m$ were found to give the best agreement between the three methods. Table 3.3 shows the determined values of the bed shear stress from all three sources. The last column indicates the largest error between τ_{lc} and the other two values. τ_{vp} has been calculated by means of the velocity profile (Figure 3.8) and the law of the wall (Equation (2.37)). More detailed steps of the iteration can be seen in Appendix D.

u_{flow} [m/s]	$\tau_{dp,b}$ [Pa]	τ_{lc} [Pa]	τ_{vp} [Pa]	Max error [%]
2.0	12	12	12	0
3.0	24	26	28	8
4.7	59	62	65	5

Table 3.3: Measured bed shear stress from three sources at three flow velocities.

In Figure 3.6 the measured differential pressure per meter has been plotted versus time at a flow velocity of 2 m/s. This is to show that the bed shear stress plot (u_{flow} = 2m/s) in Figure 3.7 corresponds. The dp/dx plots for the other velocities also correspond with the bed shear stress plots, however they are not shown because the focus is on bed shear stress.
The values of $\tau_{dp,b}$ in Figure 3.7 are calculated with the method of Pugh & Wilson (1999) as described in (Paragraph 2.2.2). What can be seen from Figure 3.7 is that the values of $\tau_{dp,b}$ from each of the dp sensors start

to separate as the flow velocity increases. It is expected that this is due to the development of the flow. The entrance length of the flow increases with the flow velocity, therefore the measurement of the sections closer to the entrance (closer to dp port 1) are probably influenced by the less developed part of the flow. Since the boundary layer will be smaller in the underdeveloped part of the flow, the shear stresses will be lower too. The values for $\tau_{dp,b}$ in Table 3.3 all correspond to the longest section (1-5, purple lines).

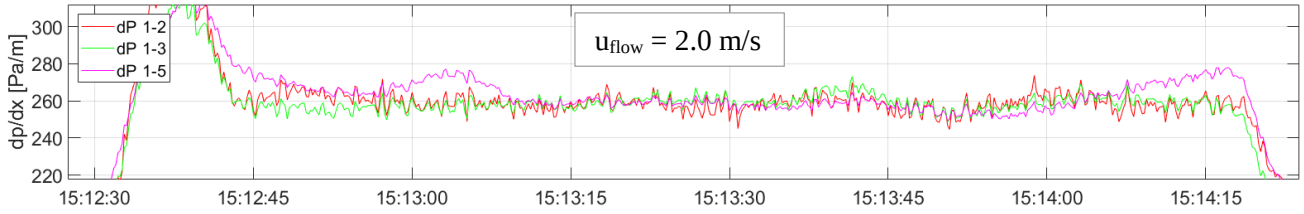

Figure 3.6: Measurement of differential pressures versus time. Measurement done at an average flow velocity of 2.0 m/s

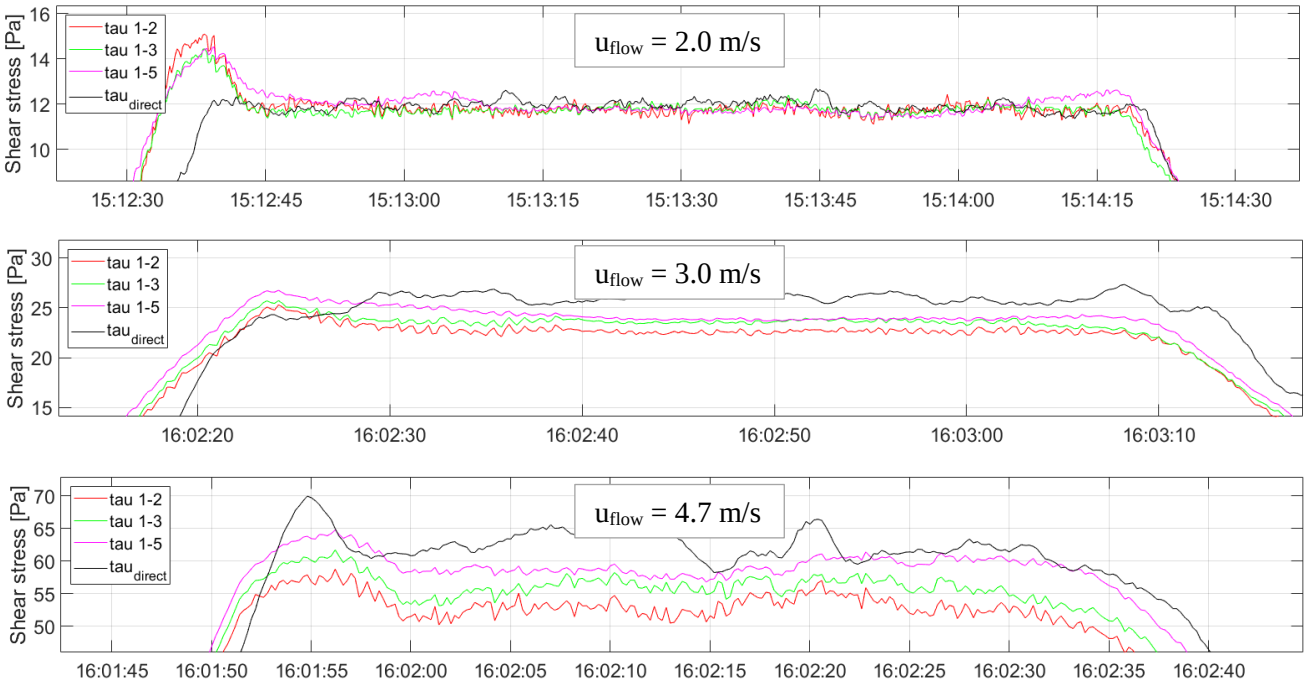

Figure 3.7: Measurement of shear stress versus time. The black line indicates the directly measured bed shear stress (load cell). The colored lines are the calculated stresses from the measured dp. Measurements done at average flow velocities of 2.0 m/s, 3.0 m/s and 4.7 m/s from top to bottom.

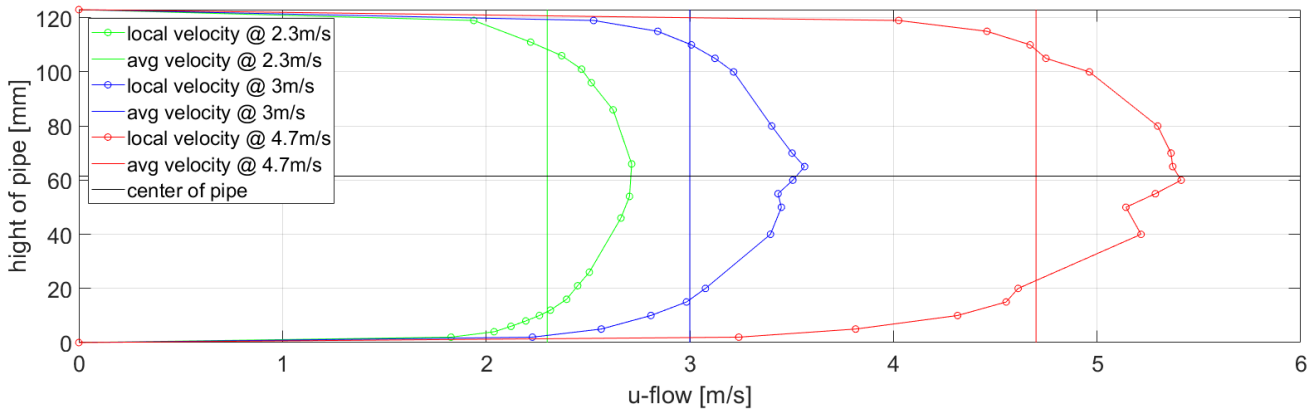

Figure 3.8: Vertical velocity profile measured at a flow of 2.3 m/s, 3m/s and 4.7 m/s

In Figure 3.9 the measured shear stress values have been plotted versus the flow velocity. It can be seen that the three methods of measuring the bed shear stress as mentioned above (BOKA, 2019) match well. For this reason

the datasets belonging to the different measurement methods will be combined and henceforth be referred to as one. Also, the measurements of BOKA (2019) and Van Rijn (1984) seem to align, meaning that one can reliable compare the results of both studies. In addition to that, calculated bed shear stresses with the CFD solver 2DV (Appendix A) align with the measurements of BOKA (2019).

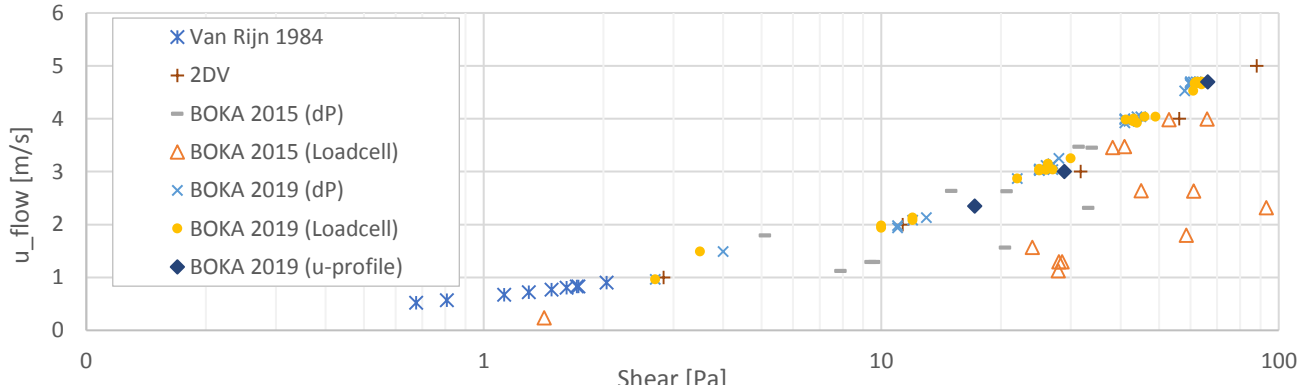

Figure 3.9: Bed shear stress versus flow velocity for several sources.

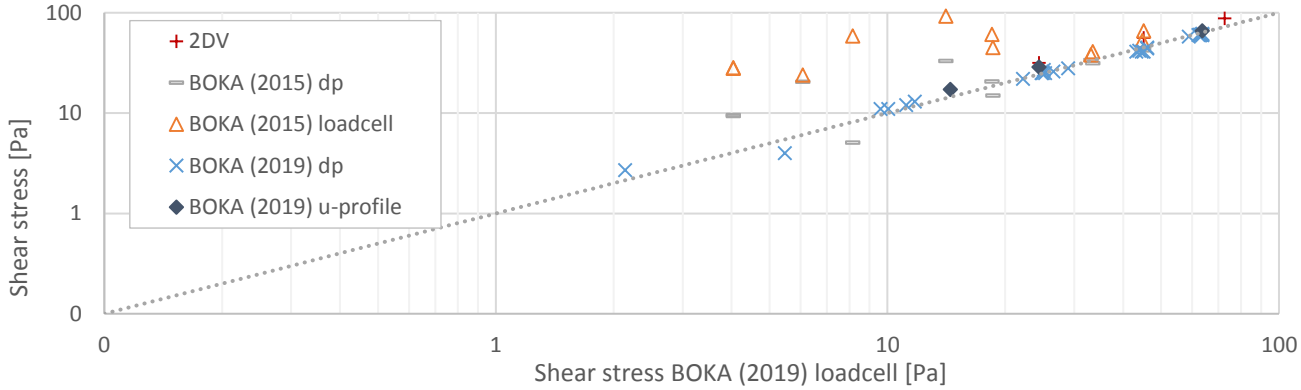

Figure 3.10: Bed shear stress of several sources compared to bed shear stress of BOKA (2019) loadcell

What is noticed from Figure 3.9 is that the measurements of the preliminary study (BOKA 2015) have a larger error margin. This was known at the time and has been the reason for the focus on reliable shear measurement. What must be noted is that several load cell measurements of BOKA (2019) had a relatively large error. It was noticed that the gap upstream of the shear board (Figure 3.1) was quite large. By replacing the shear board by a longer one, the error was resolved. In Figure 3.11 one can see the difference in measurement by both boards, where 'Old shear board' is the board that gave the larger error. Since the datapoints shown in Figure 3.11 are from erosion tests the data was needed for the rest of the study. Therefore, it was chosen to correct the values of 'Old shear board' so that the datapoints overlap with the other data (Figure 3.11).

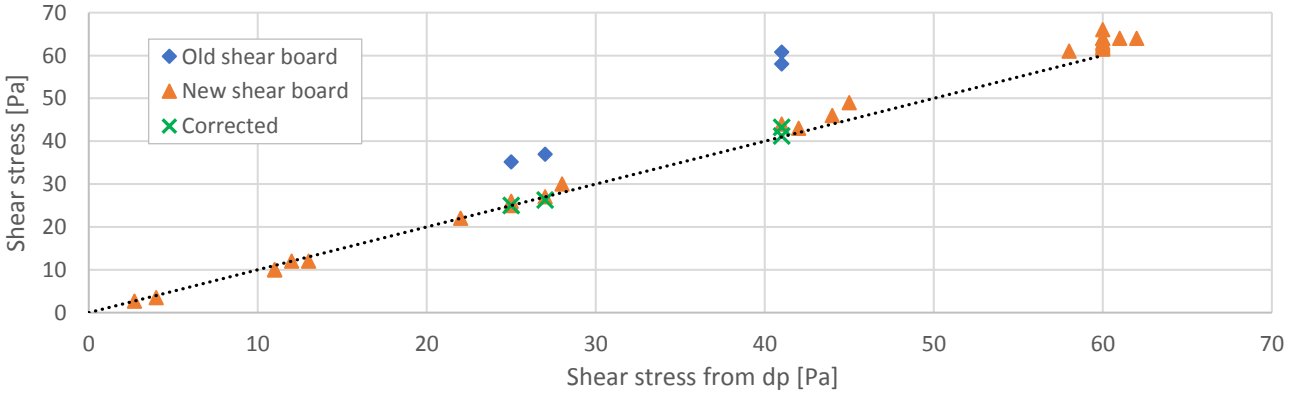

Figure 3.11: Correction of several data points from direct shear measurement.

3.6.2. Erosion velocity

The lift velocity was measured by a position sensor. By dividing small changes in distance by the elapsed time, one knows the velocity of the lift. The erosion velocity is said to be equal to the lift velocity when the eroding sand bed is horizontal (Figure 3.5b). The judgement of the flatness of the sand bed is visually made with the aid of the footage of the high-speed camera. When the lift speed is either too fast or too slow, one sees a mound or a scour pit respectively. During each measurement the lift was set to three speeds to be able to achieve all three shapes of the sand bed. In this way not only the actual erosion velocity, also the upper and lower limit of the measurement were determined (Figure 3.5a and b).

3.6.3. Porosity

The experiments were performed with a porosity ranging from 0.41 to 0.47 where the majority of experiments had a porosity of 0.43. The porosity was measured using the following equation:

$$n_0 = 1 - \frac{m_s/\rho_s}{V_m} \tag{3.2}$$

where m_s is the mass of the sand in the sample and V_m is the volume of the mixture. Since the width and length of the shaft in which the sample is prepared are fixed, the volume of the sample was determined by measuring the height of the sample. This was done with a measuring tape and has an accuracy of 1mm. The mass of the sand was measured before it was placed in the setup with a scale that has an accuracy of 1gr. It is not possible to measure the mass of the mixture once it is placed in the setup.

The measurement of the porosity has been validated with separate tests. Similar samples were made in a separate setup that has approximately the same shape as the shaft of the main test setup. In this secondary setup the weight of the mixture could be determined after the sand and water were in place. With the mass of the mixture one can calculate the porosity as follows:

$$n_0 = \frac{(m_m - m_s)/\rho_w}{V_m} \tag{3.3}$$

where m_m is the mass of the mixture. The error between the two methods can be seen in the table below. The first column shows the number of times the sample has been consolidated with the vibrator (Paragraph 3.5)

Consolidation cycle	Method Eq 3.1 [-]	Method Eq 3.2 [-]	Error [%]
0	47.7	48.9	2.5
1	45.4	45.5	0.2
2	42.4	42.8	1.1
3	40.3	40.4	0.2

Table 3.4: Porosity calculated in two ways. No vibration has been applied to consolidation cycle 0

3.7. Estimation of near bed concentration

From Equation (2.2) and (2.3) it can be seen that it is necessary to know the near bed concentration to calculate the pickup flux when the erosion velocity is measured. Since the near bed concentration cannot be measured with the setup of the current study it is estimated from the video footage. The sediment that is picked up from the bed will reach a certain height (h). The average concentration over that height is assumed to be the near bed concentration. Figure 3.12 shows the geometric relationship between the length of the bed and the height h. It is assumed that, on average, no sediment passes through the line A-C. Therefore, the flux that passes through the line A-B will also pass through the line B-C. This relation is expressed as:

$$\Phi_{AB} = v_e \cdot L \cdot (1 - n_o) = \Phi_{AC} = h \cdot u_{nb} \cdot c_{nb} \tag{3.4}$$

where $(1-n_0)$ is the concentration of the bed and u_{nb} is the flow velocity near the bed. Using the velocity profiles shown in figure Figure 3.8 the average velocity over the height h is estimated to be $u_{nb} \approx u_{flow}$.

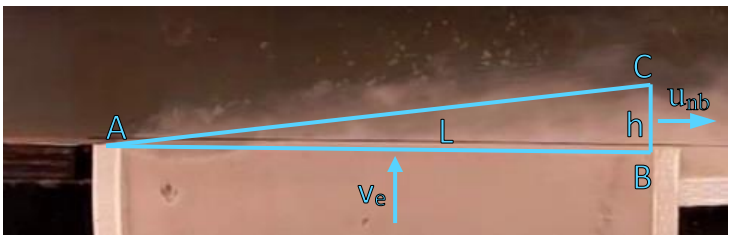

Figure 3.12: Estimation of near bed concentration

When the height h is estimated from the camera footage one can calculate the corresponding near bed concentration. In the table below the estimated near bed concentrations have been given for several bed shear stresses.

Another approach is used to confirm the estimation described above. From Equation (2.37) it can be derived that u_* is the velocity scale of turbulent bursts. Additionally, from Stokes' law, it is known that small particle diameters follow a flow very well. Therefore, it can be said that the upward velocity of the particles scales with u_* and the following relationship can be made:

$$\frac{h}{L} \propto \frac{u_*}{u} \tag{3.5}$$

When Equation (3.5) is used to substitute for h in Equation (3.4) the following equation is found:

$$\frac{v_e \cdot (1 - n_0)}{u_*} = c_{nb} \tag{3.6}$$

It can be seen from the table below that both methods of estimating the c_{nb} result in values of the same order.

u [m/s]	h [mm]	τb [Pa]	u_*[m/s]	ve [m/s]	Cnb (3.4)[-]	Cnb (3.6)[-]
1	14	2.7	0.05	0.0018	0.01	0.02
2	22	10	0.10	0.007	0.02	0.04
3	28	26	0.16	0.016	0.02	0.06
4	30	43	0.21	0.028	0.03	0.08

Table 3.5: Estimates of c_{nb} corresponding to different flow conditions.

3.8. Results

In this paragraph the most important results are discussed with the aid of graphs. Appendix B shows the results of all measurements in tables.

3.8.1. Bandwidth of measurement

As described in the previous paragraph the upper and lower limit of the measurement of v_e were determined during the experiments. Table 3.6 shows measured values of the erosion velocity with the corresponding error, which is determined from the largest difference between v_e and either of the limits. In Figure 3.13a the actual datapoints of v_e and the limits can be seen.

u_{flow}	Shear stress [pa]	v_e [mm/s]	Error [%]	Bandwidth [mm/s]
1.5	3.5	4	± 13	3.5 – 4.5
2	10	7	± 21	5.5 – 8.5
4	43	28	± 21	22 – 34
4.7	62	29	± 24	24 – 36

Table 3.6: Measurement error corresponding to different shear stresses

3.8.2. Porosity

In a study of Roberts (1998) it has been shown that the porosity has an influence on the erosion velocity. Therefore the measurements of the current study have been performed at three values of porosity: n_0=0.47, n_0=0.43 n_0=0.42. During the experiments it was noticed that the lift was not powerful enough to overcome the friction between the sand bed and the lift-shaft at values of n_0<0.42. Therefore, unfortunately only one datapoint could be used for that specific value of porosity.

The data shows a very small influence of porosity. However, the measurements of the three porosities lay within the error margin of v_e (Figure 3.13b). Therefore, the difference between the measurements could be due to the accuracy of the measurement.

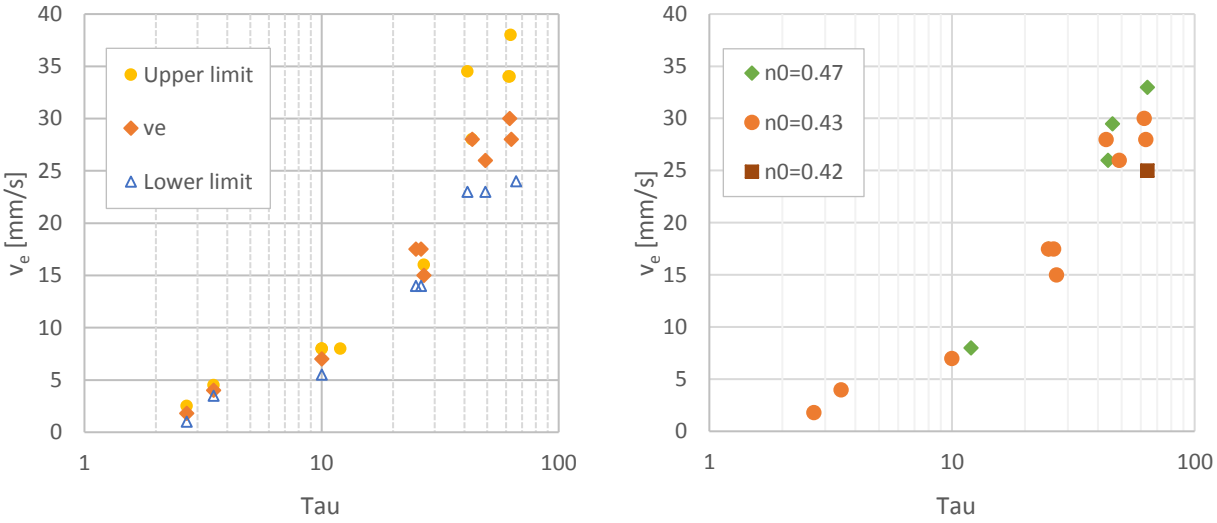

Figure 3.13: a) Upper and lower limit of measurement of erosion velocity. All data points correspond to n0 = 0.43

b) Erosion velocities corresponding to different porosities.

4. Analysis

All the data and pickup functions that have been compared in this study can be seen in Figure 4.1. From this plot the following observations can be made:

I. The data of the current study does not match the data of Bisschop (2018).
II. The pickup functions of Fernandez Luque (1974), Van Rijn (1984) and Roberts (1998) *over*estimate the pickup according to the data of the current study
III. The correction of Van Rhee (2010) and the pickup function of Van Rijn (2018) *under*estimate the pickup according to the data of the current study.
IV. The correction of Van Rhee (2010) and the pickup function of Van Rijn (2018) *over*estimate the pickup according to the data of Bisschop (2018)
V. Although different, the pickup functions of Van Rhee & Talmon (2010) and Winterwerp (1992) seem to match the data of Bisschop (2018).

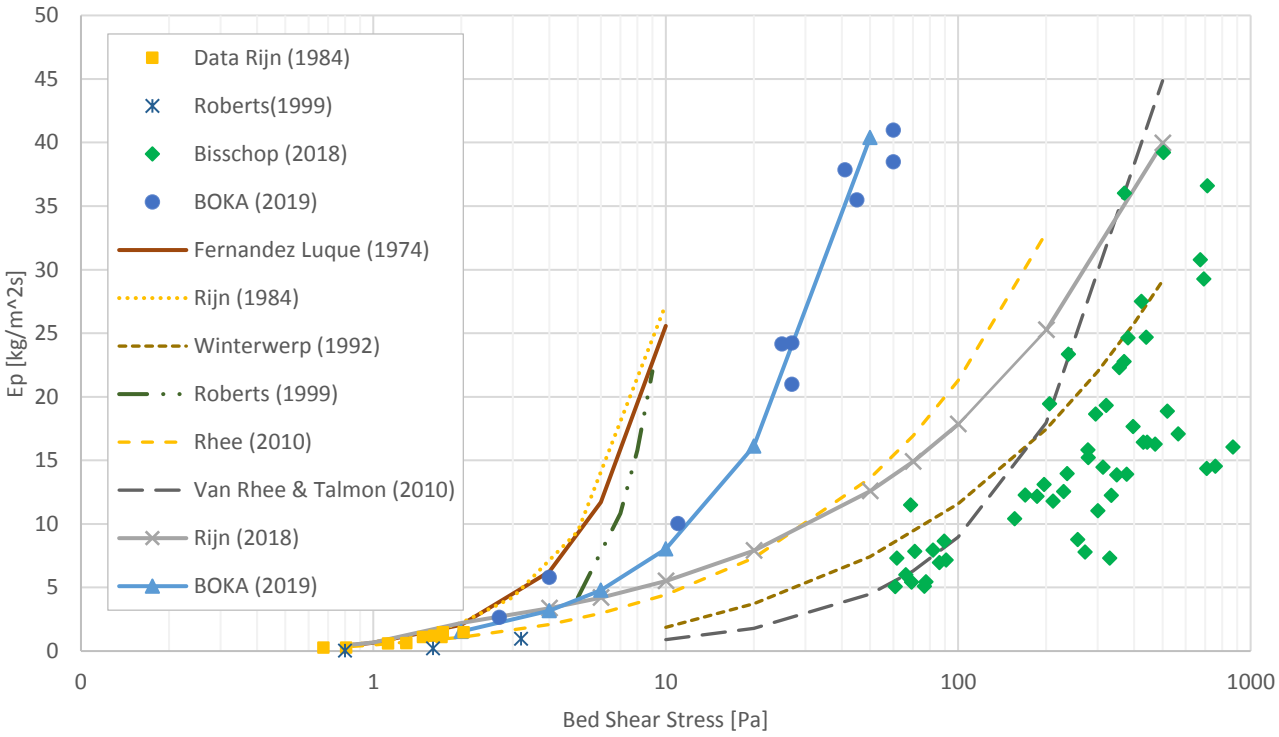

Figure 4.1: Data and functions compared in this study.

The pickup function of Cheng (2016) is of interest to the present study since the experiments were done in very similar experimental setups and the study is relatively recent. However, the experiments of Cheng (2016) were limited to flow velocities of 1 m/s ($\tau < 2$). In addition to that, Cheng (2016) mentions that his experiments cannot be well predicted by the function of Van Rijn (1984), even though Cheng (2016) based his experiments on the study of Van Rijn (1984). Therefore, the pickup function of Cheng (2016) is not considered during the overall comparison, but is compared separately in Appendix E.

This chapter will start with the demonstration of the fact that the empirical "constants" of the existing pickup functions are, in fact, not yet constant. This means that one or more processes are not yet taken into account. Next, the influence of the bed properties on the pickup flux will be discussed. After that, the reader is shown that the presence of the critical shields number in the denominator of the transport term T might be incorrect. Furthermore, the complexity of the difference between bed shear stress above a fixed bed and above a mobile bed is discussed. As can be seen from the plot in Figure 4.1, at a certain shear stress value, the measured pickup

by BOKA (2019) is much higher than that of Bisschop (2018). A difference is expected, however, not a difference as large as can be seen in the figure. The difference is present even though both studies focus on a similar velocity range. However, the experimental setups of the two parties have two crucial differences:

a) The bed shear stress in the setup of Bisschop (2018) is measured above a mobile bed and the bed shear stress in the setup of BOKA is measured above a fixed bed.
b) The sand bed of Bisschop (2018) is 6.25 m long and the sand bed of BOKA (2019) is 0.2 m long. Therefore, there will be a significant c_{nb} (Paragraph 2.1.7) over the eroding bed of Bisschop (2018) and a negligible c_{nb} over the bed of BOKA (2019).

The effect of the near bed concentration is discussed as well, after which a new pickup function presented.

It must be noted that the data of Bisschop is produced with values of porosity with a range of $0.42 < n_0 > 0.44$, while the data of BOKA (2019) only corresponds to a porosity of $n_0 = 0.43$. Bisschop (2018) shows that the effect of porosity is negligible. Also, when the same graph is plotted including the values of porosity, no pattern can be recognized (Appendix C).

4.1. Original fit

The pickup function of Van Rijn (1984) does not match with the data of BOKA (2019). The function was tuned to match the original data of Van Rijn (1984), which was measured at low flow velocities (defined as a flow with $\theta < 1\ Pa$ which corresponds to $\tau < 2\ Pa$). As can be seen in Figure 4.2 this fit is not perfect, but for practical purposes it has been proven to be close enough.
Arguably the mismatch with BOKA (2019) is due to the fact that Van Rijn (1984) did not have the data at higher shear stresses to fit the function correctly. With the current data, one could simply change the empirical constants to match both the original data of Van Rijn (1984) and the data of the current study (Figure 4.2 and Figure 4.3). In Equation (4.1) the n parameter (Paragraph 2.1.5) has been reduced. With this adjustment, neither the original data nor the data of the current study fit well, therefore, the m parameter is also adjusted (Equation (4.2)). Equation (4.2) matches the data of both studies well, however, the fact that the constants need to be changed for different experiments suggests that not all physical processes are incorporated in the equation.

$$\phi_p = 0.00005 \cdot D_*^{0.3} \cdot \left(\frac{\theta - \theta_{cr}}{\theta_{cr}}\right)^{1.5} \tag{4.1}$$

$$\phi_p = 0.00080 \cdot D_*^{0.3} \cdot \left(\frac{\theta - \theta_{cr}}{\theta_{cr}}\right) \tag{4.2}$$

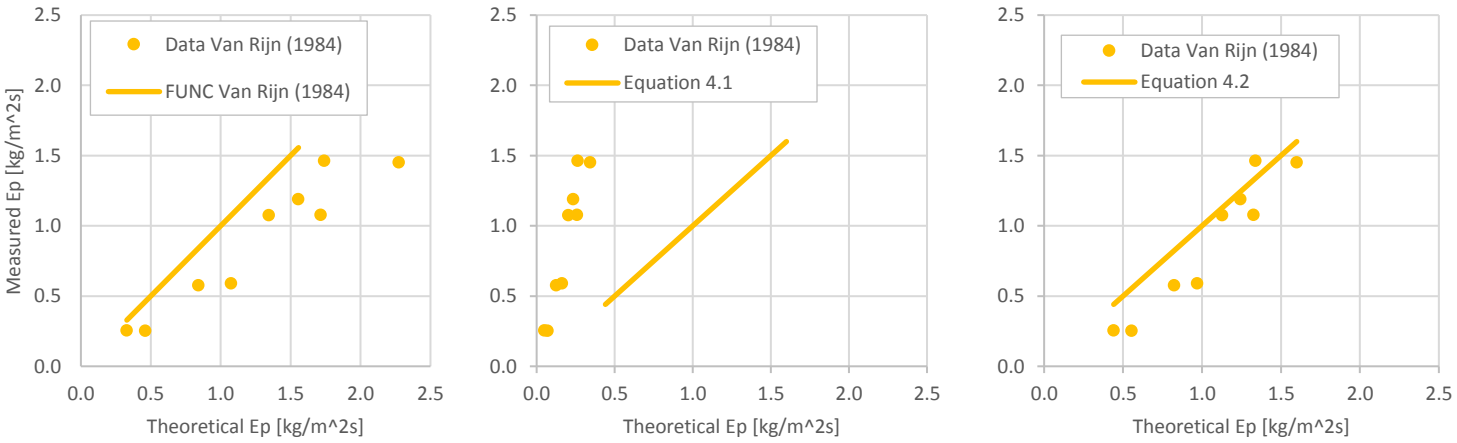

Figure 4.2: Data Van Rijn (1984) compared to Equation 4.1 and 4.2. $0.6 < \tau > 2$

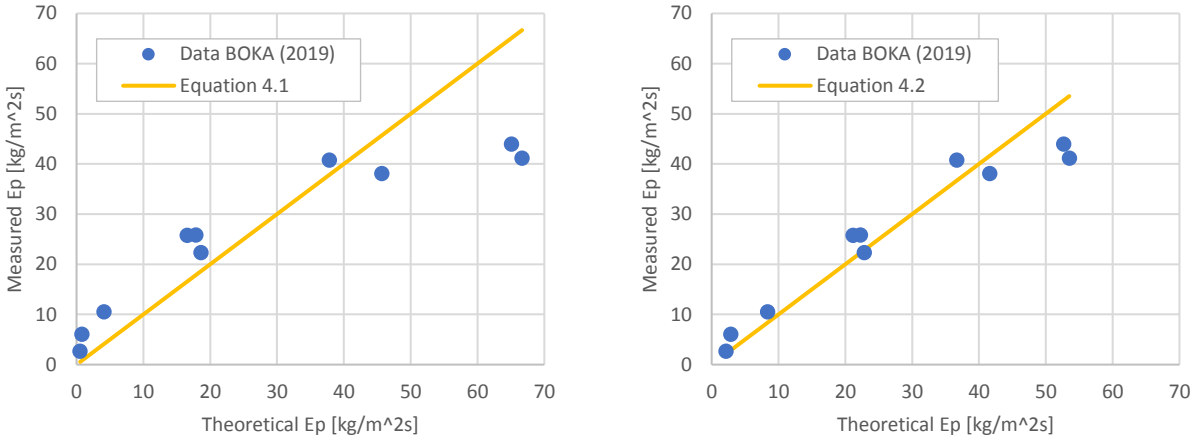

Figure 4.3: Data of Boka (2019) compared to Equation 4.1 and 4.2 $2 < \tau > 60$

4.2. Bed properties

In the study of Van Rhee (2010) a correction for the function of Van Rijn (1984) is suggested that takes the influence of the bed properties into account. As described in Paragraph (2.1.6) the critical shields value has been corrected to include the effect of an inward hydraulic gradient due to dilatancy. The correction of Van Rhee (2010) was validated with data produced during the studies of Bisschop (1993) and Roberts (1998). For both studies the c_{nb} was negligible and the bed shear stresses (and thus flow velocities) where higher than that of Van Rijn (1984) (up to 6 Pa). The current study, however, has produced data with much higher bed shear stresses (up to 60 Pa). With this data one can see (Figure 4.5) that the correction of Van Rhee (2010) largely underestimates the pickup, although it matches the original data of Van Rijn (1984). When the function is compared to the data of Bisschop (2018), it is an *over*estimation, however.
In Paragraph 3.6.3 it was shown that the porosity of the prepared sand bed has an influence on the erosion velocity during the experiments of this study. In Table 4.1 the difference between v_e (and corresponding E_p) of Van Rhee (2010) and BOKA (2019) can be seen. The influence of porosity is larger in the correction of Van Rhee (2010) than in the data of BOKA (2019).

	Data BOKA (2019)				Van Rhee (2010)			
n_0	v_e		Ep		v_e		Ep	
[-]	[mm/s]	[%]	[kg/m^{2}s]	[%]	[mm/s]	[%]	[kg/m^{2}s]	[%]
0.42	25	32	38	34	11	55	16	50
0.47	33		51		17		24	

Table 4.1: Influence of porosity on correction of Van Rhee (2010) at 62 pa.

To be able to reduce the influence of porosity and permeability a damping factor δ is used in the corrected shields number of Van Rhee (2010) (Equation (4.3)). It has been found that a damping factor of $\delta = 0.18$ results in a good fit with the data of the current study when the pickup is calculated with Equation (4.4) (Figure 4.5).

$$\theta''_{cr} = \theta_{cr}\left(\frac{sin(\phi-\beta)}{sin\,\phi} + \delta \cdot \frac{v_e}{k_l} \cdot \frac{n_l - n_0}{1 - n_l} \cdot \frac{A}{\Delta}\right) \tag{4.3}$$

$$\phi_p = 0.00033 \cdot D_*^{0.3} \cdot \left(\frac{\theta - \theta''_{cr}}{\theta''_{cr}}\right)^{1.5} \tag{4.4}$$

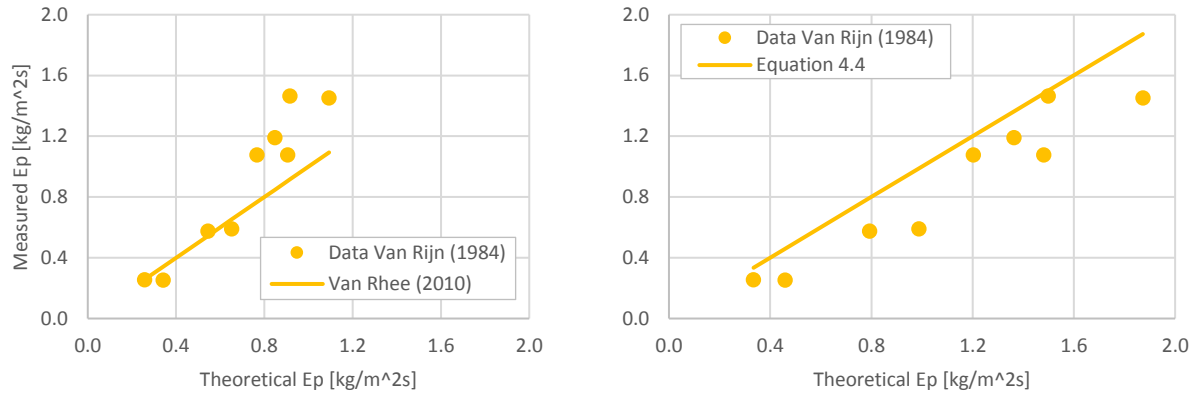

Figure 4.4: Data Van Rijn (1984) compared to Van Rijn (2010) and Equation 4.4. $0.6 < \tau > 2$

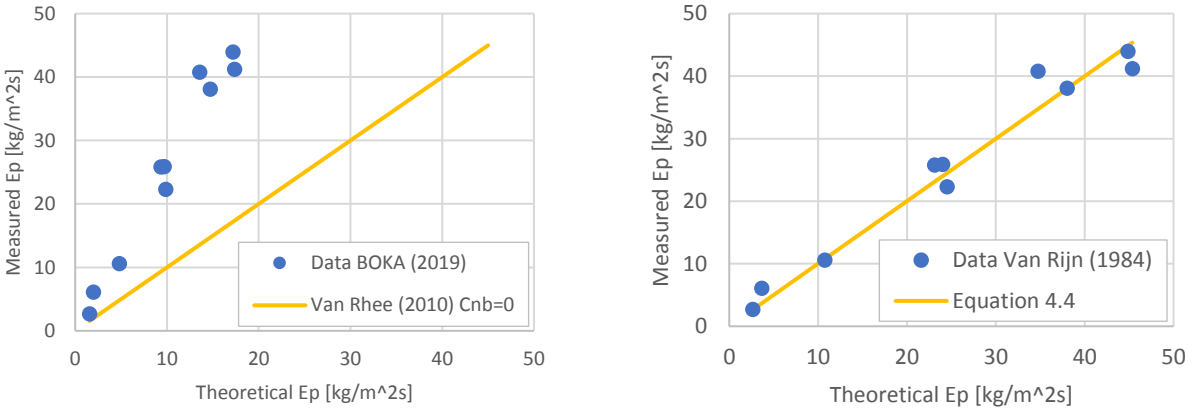

Figure 4.5: Data of Boka (2019) compared to Van Rhee (2010) and Equation 4.4. $2 < \tau > 60$

4.3. Transport term

In the transport term T of Van Rijn (1984) the critical shields number is in the denominator. This value is the minimum value necessary to initiate motion of the sediment (Paragraph 2.1.4). In other words, it is a parameter that applies to low velocities (or low shields values). However, when the critical shields number is in the denominator, it will have influence over the entire range of θ. Arguably, the parameter for initiation of motion should become less and less important as the shear stress (or shields number) increases.

In the case of Van Rijn (1984) (Equation (2.24)), one could argue that this presence of the critical shields number in the denominator is responsible for the overshoot in pickup as the shields value increases. Additionally, the influence of dilatancy currently seems to be too strong at higher shields values (Paragraph 4.2). Removing the critical shields value from the denominator would solve the mentioned problems, while the critical shields number, and thus the effect of dilatancy, still play a role when θ is in the order of magnitude of θ_{cr}. It must be noted that when the critical shields number is removed from the denominator, the damping factor δ should not be used in the adjusted critical shields parameter of Van Rhee (2010).

In the studies of Fernandez Luque (1974), Winterwerp (1992) and Van Rhee & Talmon (2010), pickup functions are given where there is no division by the critical shields number. The last two functions fit the data of Bisschop (2018), which was produced with flows of high velocity, well (Figure 4.1). Once again this proves that not all processes are fully understood and that the pickup functions are missing one or more terms. The effect of dilatancy for example is not incorporated in either of the functions of Winterwerp (1992) and Van Rhee & Talmon (2010).

4.4. Bed shear stress

The pressure delivered by the pump is the driving force that produces a flow velocity and subsequently shear stresses. However, interaction with the bed influences the value of the shear stress as well. From the comparison of the present study it can be seen that the bed shear stress is significantly higher over a mobile bed with a developed concentration profile than over a fixed bed with clean water. As explained in Paragraph (2.2.3) the

shear stress over a mobile bed is most likely higher due to more factors than just picking up of grains. Since In Figure 4.6 the measured shear stress of Bisschop (2018) and the present study have been plotted versus the flow velocity. It can be seen that at a certain flow velocity the shear stress measured by Bisschop (2018) is much higher than that of BOKA (2019). It is also clear that the shear stress measured by Bisschop has a larger spread. If it is assumed that the measurement of Bisschop (2018) is accurate (dp measurement over 3m), the spread suggests that there is a process influencing the bed shear stress which is still unaccounted for.

Bisschop (2018) gives an empirically found function (Equation (2.44)) for the roughness factor above the eroding bed (λ_b) in his experimental setup. This roughness factor describes an effective roughness as explained in Paragraph (2.2.3) and can be used in Equation (2.16). The shear stresses calculated with this roughness factor have been plotted in Figure 4.6 as well. It can be seen that the match with the data of Bisschop (2018) is not perfect. In Figure 4.7 one can see the theoretical bed shear stress calculated with the mentioned function compared to the bed shear stress that was actually measured. The values inside the bubbles in the plot represent the porosity in percentage. The graph suggest that a looser sand bed leads to a higher bed shear stress.

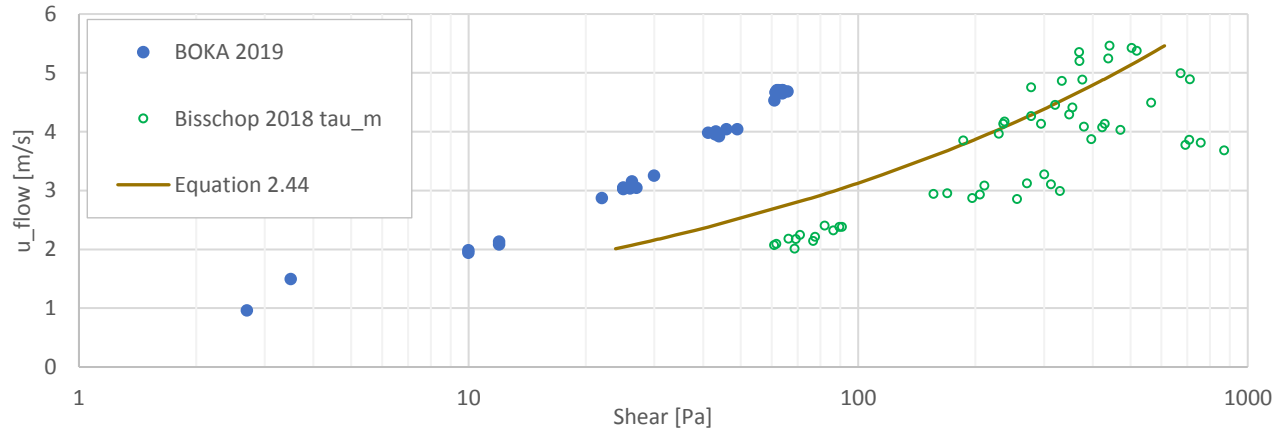

Figure 4.6: Shear stress comparison between BOKA (2019) and Bisschop (2018). Note that u_{flow} is on the y-axis

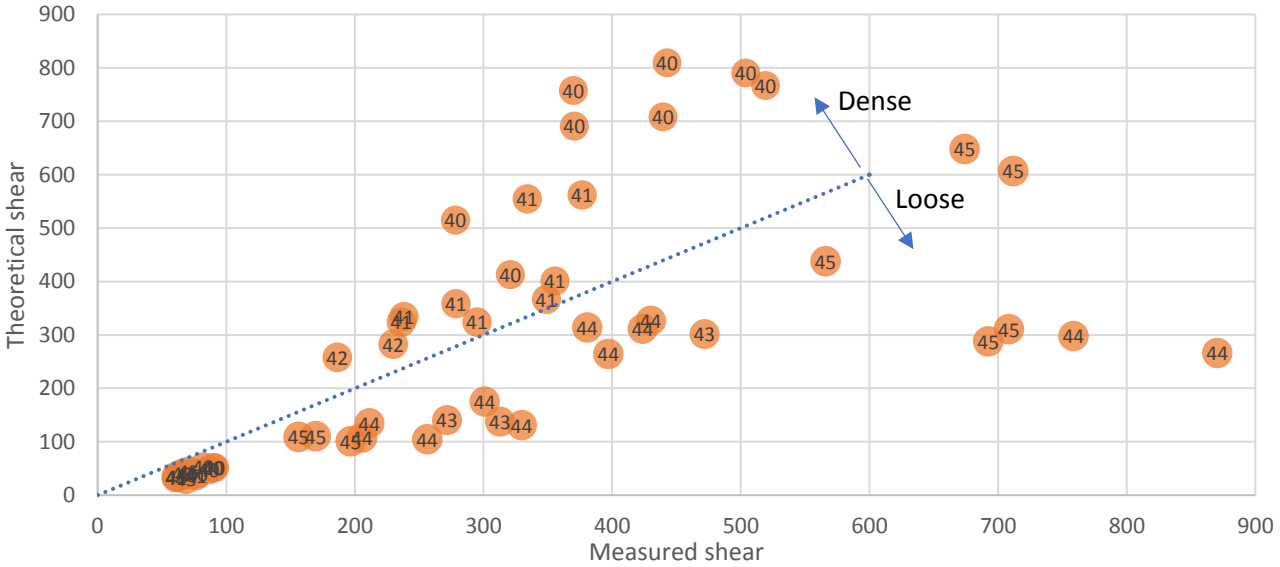

*Figure 4.7 Measured bed shear stress by Bisschop (2018) versus the theoretical bed shear stress calculated according to the roughness function (Equation (2.44)**Error! Reference source not found.**) given by Bisschop (2018). The number in the bubbles r epresents the porosity (in percentage) of the sand bed.*

To be able to link the pickup to the actual shear stress over a mobile bed would be ideal. However, it is clear that the bed shear stress over a mobile bed is not yet fully understood. Therefore, the present study suggests to keep using the fixed-bed shear stress when predicting the pickup of sand. This is an engineering approach to work around the complexity of the eroding-bed shear stress.

To be able to compare the data of Bisschop (2018) and the present study, a bed shear stress needs to be found corresponding to the pickup values of Bisschop (2018). The method of Pugh & Wilson (1999) was used in the same way as in the present study where a fixed bed with a roughness height of $k_{r,b} = 2 \cdot d_{90}$ and a wall roughness of $k_{r,w} = 0.05$ were used. Using the correct dimensions of the setup of Bisschop (2018) a roughness factor of $\lambda_b = 0.24$ was found. The same value is used for the bed shear stress of the present study. Once again the shear stresses haven been shown as a function of flow velocity in Figure 4.8, now with the addition of the calculated bed shear stress over a fixed bed (τ_f) for the data of Bisschop (2018).

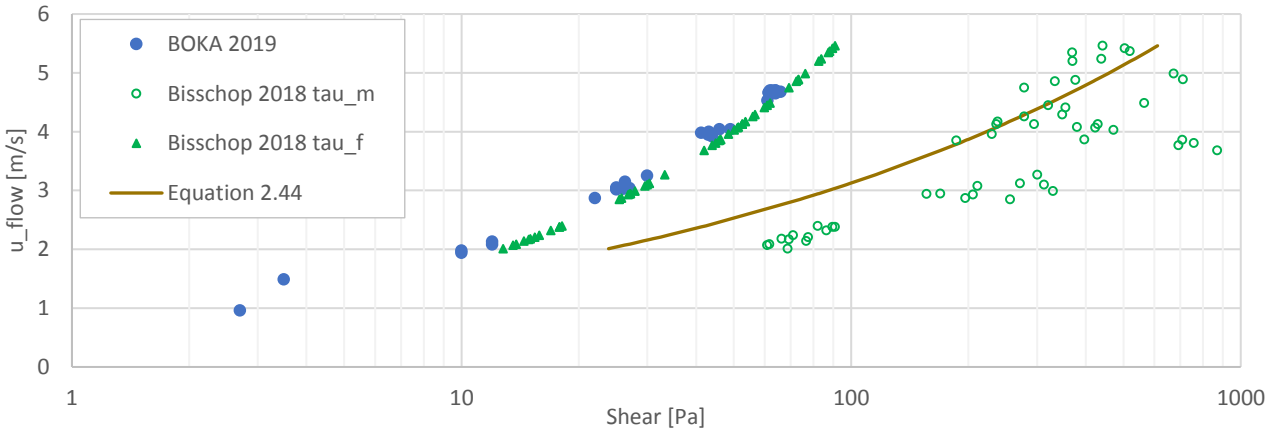

Figure 4.8: Shear stress comparison between BOKA (2019) and Bisschop (2018). Note that u_{flow} is on the y-axis

When the pickup values of Bisschop (2018) are plotted (Figure 4.9) as a function the new shear values, it can be seen that the data lies much closer to that of the present study. At a certain shear value the pickup measured by Bisschop (2018) is still lower, however a mismatch of this order is to be expected and is discussed in the next paragraph.

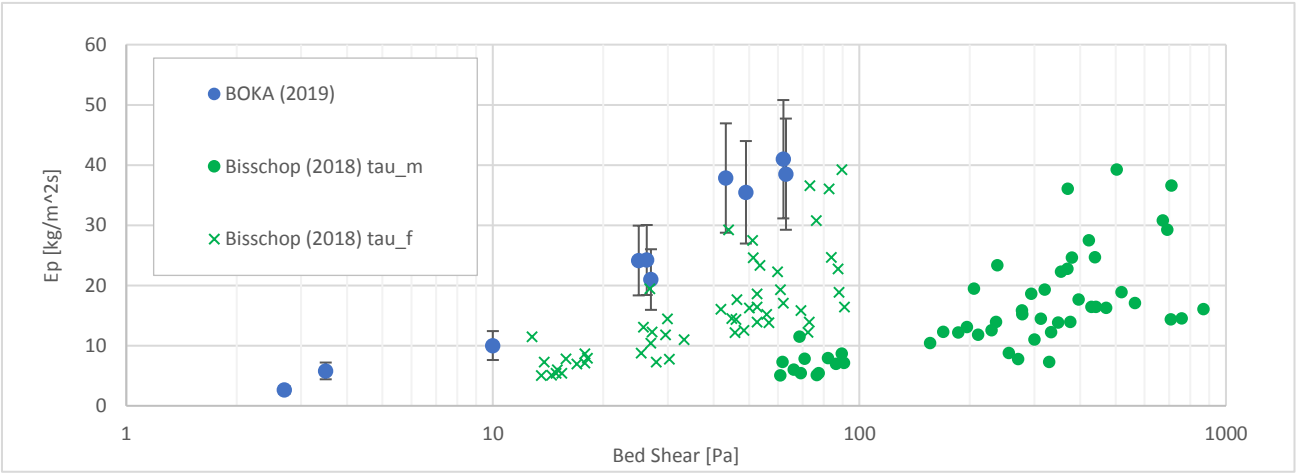

Figure 4.9: Data of Bisschop (2018) with shear values calculated for a fixed bed. Error bars showing worst case of 24%

4.5. Near bed concentration

Since sediment is transported along the sand bed, the near bed concentration will be low at the start of the bed and become higher in the direction of the flow. At a certain point the pickup and sedimentation (Paragraph 2.1) reach an equilibrium and the near bed concentration reaches a maximum (Figure 4.10).

The pickup flux measured by Bisschop (2018) was measured in the middle of a long bed (6.25 m), where the near bed concentration is relatively high ($c_{nb} \approx 0.2$). Therefore, the pickup of Bisschop (2018) can be referred to as hindered pickup (Paragraph 2.1.7). BOKA (2019) measured the pickup over 0.2 m, where the near bed concentration is still relatively low ($c_{nb} \approx 0.03$, Paragraph 3.7). So low, in fact, that the effect of hindered erosion is negligible. Therefore, the pickup measured by BOKA (2019) is considered to be *un*hindered pickup.

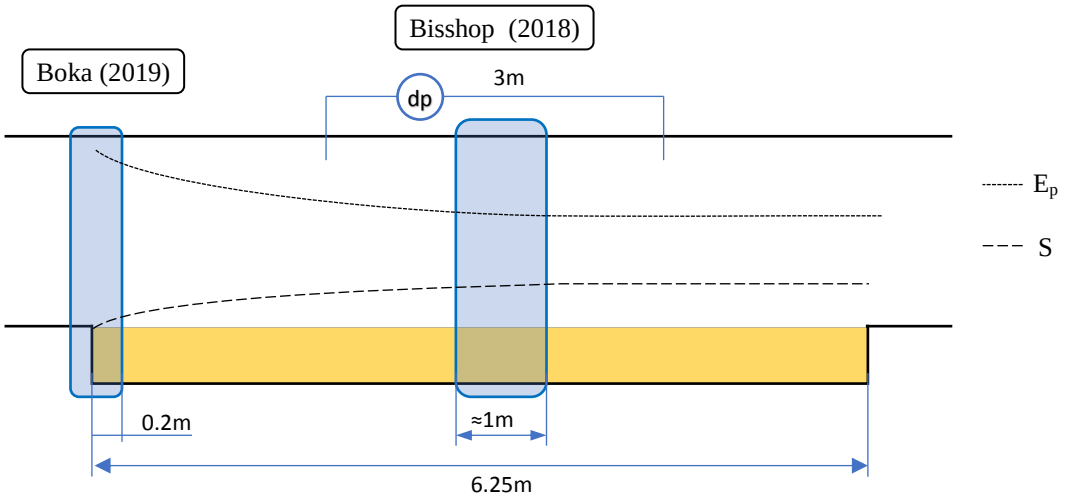

Figure 4.10: Decreasing E_p over length

Now the data of Bisschop (2018) that has been modified for the shear can be further adjusted to represent a value that corresponds with *un*hindered pickup. The correction term of Van Rhee & Talmon (2010) (Equation (2.36)) has been used to convert the hindered values of Bisschop (2018) into unhindered values with the corresponding near bed concentration. In that way, it can be compared to the data of BOKA (2019) (Figure 4.11). In this graph we see a reasonable match that, for an engineering approach in dredging applications, is acceptable.

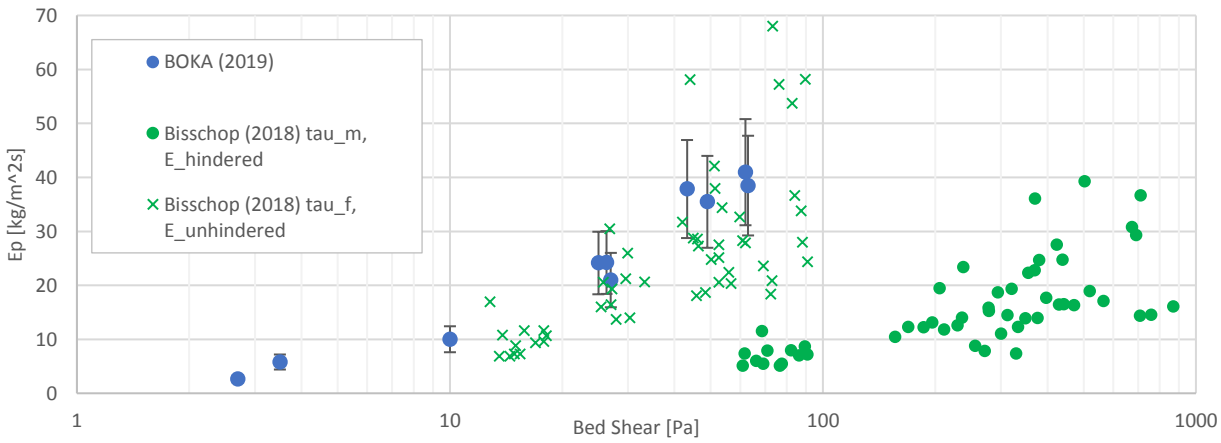

Figure 4.11: Bisschop (2018) adjusted over shear and pickup. Error bars showing worst case of 24%

4.6. New pickup function

By applying all that has been stated above, a new pickup function is suggested. The bed shear stress used to calculate the pickup should be corresponding to a shear stress of a fixed bed with a roughness corresponding to the grain diameter.
The critical shields number has been left out of the denominator in the transport function T. As described before, this will solve the problem of the overshooting in the case of Van Rijn (1984) (Equation (2.24)) and will weaken the influence of dilation reduced erosion, which is too strong in Equation (2.27) (Van Rhee, 2010). Also, the factor for hindered erosion as mentioned in Paragraph (4.5) has been included in the function.
As shown in Paragraph (4.1) the constants of the current pickup functions are actually not yet constant. Therefore, the constants in the new function have been adjusted to fit the data of BOKA (2019). Equation (4.5) shows the newly proposed function, which can be seen in Figure 4.12.

$$\phi_p = 0.011\, D_*^{0.3}(\theta - \theta'_{cr}) \cdot \frac{1 - n_0 - c_{nb}}{1 - n_0} \tag{4.5}$$

What must be noted is that the function does not seem to match well with the data of Bisschop (2018) (hindered, and fixed-bed shear stress), even though a near bed concentration of 0.2 has been entered into the function. One could simply add a power to the hindered erosion factor to make the data fit (it is found that a power of 1.8 fits well). However, this does not explain the physics behind the near bed concentration. Also, the data of Bisschop (2018) presented in Figure 4.12 has been given new values of the bed shear stress as described in Paragraph 4.4. It could also be that this representation of the data is not accurate and that the comparison is not valid. It is recommended to produce more data with long sand beds where a near bed concentration will be present. With this data one could find the correct way to include the influence of the near bed concentration.

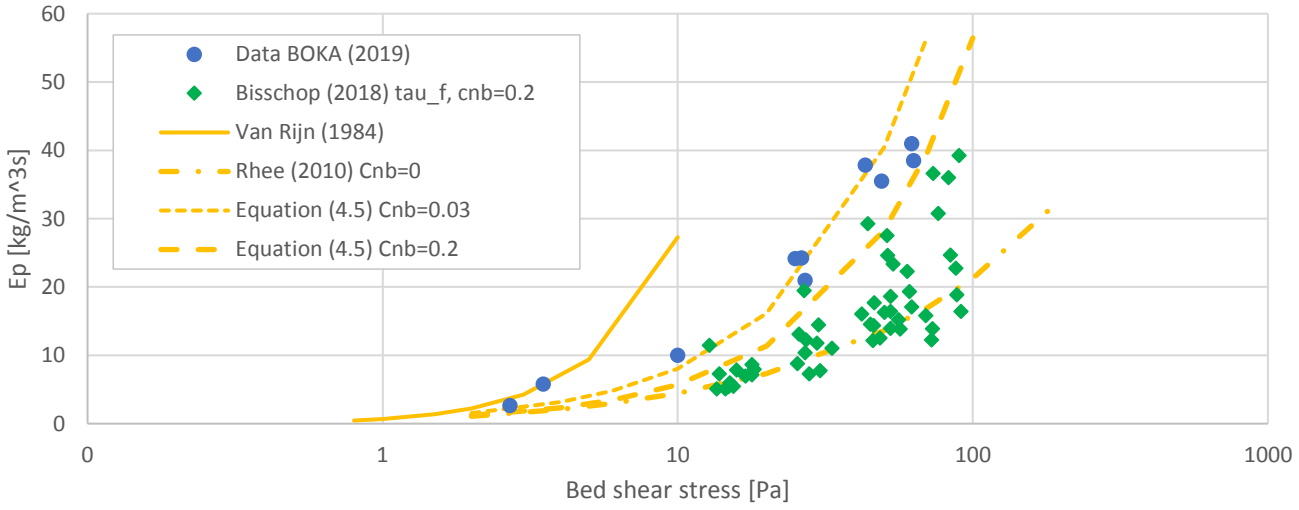

Figure 4.12: New pickup function compared to data and existing functions

5. Conclusion

As part of the present study a dataset has been produced with flow velocities ranging from 1 to 4.7 m/s. Since the bed shear stress is such an important parameter, the accuracy of this parameter was a main focus. The bed shear stress was determined with three different methods with which could be determined that the values are consistent (error up to 8%).

The present study has confirmed that the existing pickup functions are not yet complete. Although the pickup function of Van Rijn (1984) is validated to data at low flow velocities, the function largely overestimates the pickup at high flow velocities compared to the data of the current study. In addition to that, the correction of Van Rhee (2010) largely underestimates the pickup compared to the data of the current study. This is the case even though the correction of Van Rhee (2010) was validated to the data of Roberts (1998) who used a very similar setup to BOKA (2019). The experiments of Roberts (1998) were done at higher velocities than the experiments of Van Rijn (1984), however, not as high as the current study, which shows the underestimation of the correction of Van Rhee (2010).

Also, it is argued that the critical shields number, which is a low velocity parameter, should not be in the denominator of the transport parameter T. Having it in the denominator will give it influence over the entire range of θ. It is expected that this is the main reason that the pickup function of Van Rijn (1984) overestimates the data of the current study. Also, since the correction of Van Rhee (2010) is built into the critical shields parameter, the fact that the function with the correction of Van Rhee (2010) underestimates the pickup compared to the current study, is most likely due to the presence of the critical shields number in the denominator.

It has been determined that there is a completely different relation between the pickup and bed shear stress when measured above a mobile bed or above a fixed bed. It is believed that only a part of bed shear stress measured above a mobile bed is induces pickup. Therefore, the data of Bisschop (2018) cannot be directly compared to the data of BOKA (2019). The bed shear stress above a mobile bed is much higher than over a fixed bed. The main reason for the large gap between the data of Bisschop (2018) and BOKA (2019) is believed to be the presence of a sheet layer. Most of the shear stress produced by the flow goes into the movement of this layer and not into picking up of the grains.

The way to compare the two studies is by calculating bed shear stresses corresponding to a fixed bed with a roughness corresponding to the grain diameter. This comparison shows that with the presented method and function the pickup of sand can be predicted at high flow velocities.

One can chose to use different pickup functions with different types of shear stress depending on the application. It is expected however, that with more knowledge of the development of shear stress due to erosion, a universal pickup function will be found.

6. Discussion and Recommendations

General recommendations
It is known that extrapolation of empirical functions is risky. The present study has confirmed this for the use of pickup functions. As described in the introduction, flows up to 50 m/s can be produced by water jets during dredging processes. Since the experiments of this study were limited to 4.7 m/s it is advised to do further research into the erosion process in the presence of water jets.

Until now there is no certainty on the relation between pickup and the shear stress over a mobile bed. In the current study it is suggested that the bed shear stress over a mobile bed induces more processes than pickup and must therefore, be higher than above a fixed bed before pickup occurs. It is recommended to further investigate the shear stress over a mobile bed where one can accurately measure the porosity of the sand bed, the background concentration of the flow and the near bed concentration.

In the present study and all of the studies that have been mentioned the settling flux has been calculated with equation (2.3) and the addition of hindered settling of Richardson and Zaki (1954). These equations have been defined for a stationary water column. It is strongly suspected that the presence of a (turbulent) flow will influence the settling flux significantly.

The present study, Van Rijn (1984), Roberts (1998) and Cheng (2016) have all produced erosion data with a setup that has a sediment lift. The length of these lifts (in flow direction) differ from study to study. Some are short (2 cm - 5 cm) to be able to eliminate sedimentation from the results and others are a bit longer (10 - 20 cm). It can be argued that sedimentation can take place and that a near bed concentration can develop above the longer lifts. This can influence the erosion velocity.

Improvements of the experimental setup
When the setup is used for further research it is recommended to add a pressure port downstream of the sand bed. In that way the pressure loss over a length including the sand bed can be measured. This can give more information about the bed shear stress over the mobile bed.

The motor that drives the sediment lift of the present study is technically capable of dealing with the loads due to the weight of the sand bed and the friction of the lift shaft. However, the transmission of the spindle is not optimal. To achieve the required lift speeds low flow velocities the motor has to work outside of its nominal speed range. It is recommended to select a different transmission that will allow the motor to run at higher rpm while the lift speed stays in the same range.

7. Bibliography

Bisschop, F. (2018). *Erosion of Sand at High Flow Velocities.*

Brownlie, W. R. (1981). Prediction of flow depth and sediment discharge in open channels. *Technical Report Rep. N-KH-R-43A, Keck Lab. of Hydr. and Water Resou., California Institute of Technology, Pasadena, Calif*.

Cao, Z. (1997). Turbulent bursting-based sediment entrainment function. *Journal of Hydraulic Engineering*, 129(11):1054-1056.

Colebrook, C. F. (1939). Turbulent flow in pipes, with particular reference to the transition region between the smooth and rough pipe laws. *J. Inst. Civil Eng.*, 11(4), 133-156.

Ferguson, R., & Chuch, N. (2004). A Simple Universal Equation For Grain Settling Velocity. *Journal of Sedimentary Research*.

Fernandez Luque, R. (1974). *Erosion and Transport of Bed-Load Sediment.* PhD thesis, Delft University of Technology, Delft, The Netherlands.

Gao, P. (2008). Transition between two bed-load transport regimes. *Journal of Hydraulic Engineering*.

Garcia, M. H. (2007). Sedimentation engineering: Processes, Measurements, modeling, and practice. *Manuals and reports on Engineering practice. American Society of Civil engineers*.

Greimann, B. P. (1999). Two-Phase formulation of suspended sediment transport. *Journal of Hydraulic Research*.

Miedema, S. A. (2010). Constructing the Shields curve, a new theoretical approach and its applications. *WODCON XIX, Bejing China*.

Miedema, S. A., & Matousek, V. (2014). An explicit formulation of bed friction factor for sheet flow. *Internation Freight Pipeline Society Symposium 2014.* Praha, Czech Republik: International Freight Pipeline Society.

Nobel, A. J. (2017). Erosion Velocity of Large Grains Subjected to a High Unifrom Flow Velocity. *Journal of Hydraulic Engineering*.

Pugh, F., & Wilson, K. (1999). Velocity and concentration distributions in sheet flow above plane beds. *Journal of Hydraulic Engineering*.

Richardson, J., & Zaki, W. (1954). Sedimentation and Fluidisation: Part I. *Trans. Inst. Chem. Eng.*, 32:35-53.

Roberts, J. (1998). Effects of Particle Size an Bulk Density on Erosion of Quarts Particles. *Journal of Hydraulic Engineering*.

Rowe, P. (1987). A convenient empirical equation for estimation of the Richardson-Zaki exponent. *Chem. Eng. Science*, 42(11):2795-2796.

Van Rhee, C. (2010). Sediment Entrainment at High Flow Velocity. *Hournal of Hydraulic Engineering*.

Van Rhee, C., & Talmon, A. (2010). Sedimentation and erosion of sediment at high solids concentration. *18th International Conference of Hydrotransport.* Rio de Janeiro.

van Rijn, L. C. (1984). Sediment Pick-Up Functions. *Journal of Hydraulic Engineering*.

van Rijn, L. C. (1993). *Principles of Sediment Transport in Rivers, Estuaries and Coastal Seas.* Amsterdam: Aqua Publications.

van Rijn, L. C. (2018). Modified Sediment Pick-Up Function. *Journal of Hydraulic Engineering*.

Winterwerp, J. C. (1992). Hyperconcentrated Sand-Water Mixture Flows over Erodible bed. *Journal of Hydraulic Engineering*.

Appendix A. 2DV calculation

A 2DV CFD model was used to help understand the difference between the data of Bisschop (2018) and the data of the present study. The model is represented by the sketch in the top of Figure A1. The pickup function of van Rhee (2010) is used to calculate the erosion in this model. Also the correction for the near bed concentration of Van Rhee & Talmon (2010) is used in the model.

The top surface of the sand bed in the experiments of the present study was kept at the same height by pushing the lift upwards. To mimic this process in the CFD model, the calculation module was adjusted so that the bottom cells, containing the sand bed, never emptied. In this way, sand was still transported through the model, but the shape of the bed stayed the same.

The erosion velocity was measured at different locations during the experiments of Bisschop (2018) and the present study. Bisschop (2018) had a long (6.75m) sand bed and measured the erosion velocity near the center of the bed. The present study had a short sand bed of 0.2m long, which is represented by the first 0.2 m of the CFD model. The results of the calculations with this model were used to give insight in the difference between the erosion velocity at the different locations.

The calculated bed shear stress (expressed as the dimensionless shear stress θ in the model) right before the sand bed agrees well with the measured shear stress BOKA (2019), which was also measured right before the sand bed. As can be seen in Figure A2, the calculated pickup agrees well with the pickup function of Van Rhee (2010). This is expected since the model is based on that function. What can also be seen is that both the pickup function and the results of the CFD calculation underestimate the experimental results of BOKA (2019).

Figure A1 also shows a graph of the erosion velocity versus the length of the sand bed. It can be seen that there is a significant difference in the erosion velocity at the different locations. This is most likely due to the presence of a near bed concentration. This graph gives insight into what might be happening in reality.

In the graph of Figure A1 one can also see the bed shear stress expressed as θ. It can be seen that the shear stress decreases above the mobile bed. This is not expected since Bisschop (2018) measures very high bed shear stresses during his experiments. However, the bed shear stress is calculated by assuming a fixed roughness corresponding to the grain diameter. Due to the fact that picking up the grains slows the flow down, the bed shear stress seems to decrease in this CFD model.

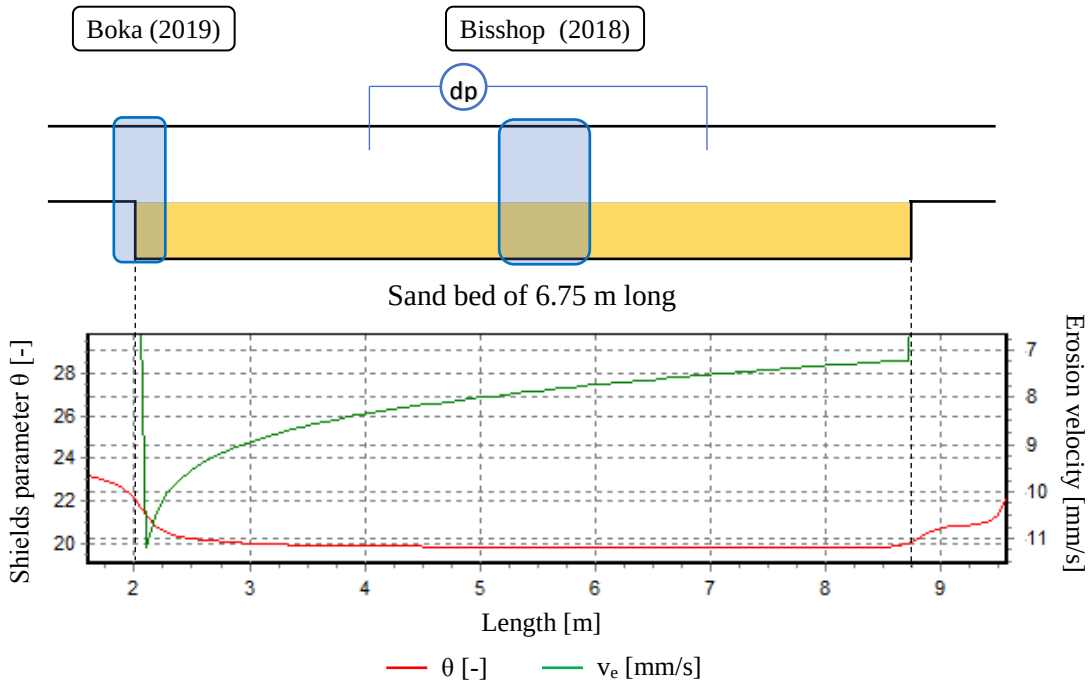

Figure A1: Plot of v_e and theta calculated with 2DV. Sand bed starts at 2m and ends at 8.75 m

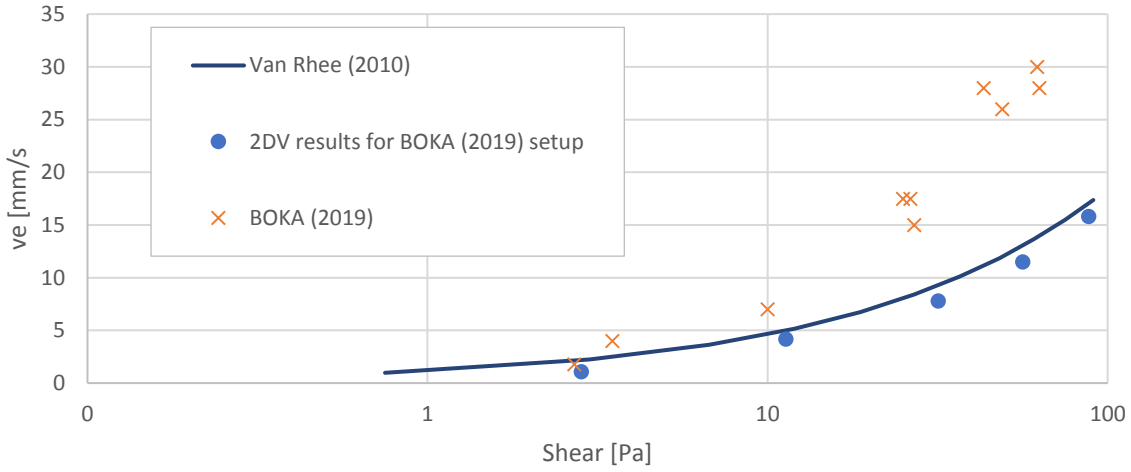

Figure A2: Erosion velocity resulting from the CFD calculation compared with the pickup function of Van Rhee (2010) and the experimental data of BOKA (2019).

Appendix B. Data

		Bed shear stress		v_e			
Test nr	**u_{flow}**	**Load cell**	**dp**	**lower limit**	**v_e**	**upper limit**	**c_{nb}**
	[m/s]	**[Pa]**	**[Pa]**	**[mm/s]**	**[mm/s]**	**[mm/s]**	**[-]**
Run 47	4.70	64	62			28	
Run 48	4.65	64	60		25		0.05
Run 49	4.67	63.9	60	23			

Table B1: Data from experiments at $n_0 = 0.42$

		Bed shear stress		v_e			
Test nr	**u_{flow}**	**Load cell**	**dp**	**lower limit**	**v_e**	**upper limit**	**c_{nb}**
	[m/s]	**[Pa]**	**[Pa]**	**[mm/s]**	**[mm/s]**	**[mm/s]**	**[-]**
Run 15	3.0	25.0	25.0	14.0	17.5		0.05
Run 16	3.2	26.3	27.0	14.0	17.5		0.05
Run 17	4.0	43.2	41.0		28.0		0.06
Run 18	4.0	41.2	41.0	23.0		34.5	
Run 19	3.1		26.0			21.0	
Run 22	3.0	27.0	27.0		15.0	16.0	0.04
Run 24	4.0	43.0	42.0			28.0	
Run 25	4.0	49.0	45.0	23.0	26.0		0.06
Run 26	2.1	12.0	13.0			8.0	
Run 27	1.9	10.0	11.0	5.5		8.0	
Run 28	2.0	10.0	11.0		7.0	8.0	0.03
Run 31	1.5	3.5	4.0	3.5	4.0	4.5	0.02
Run 38	4.7	62.6	60.0			38.0	
Run 39	4.7	62.0	60.0		30.0	34.0	0.05
Run 40	4.7	61.5	60.0			34.0	
Run 41	4.7	63.0	60.0		28.0		0.05
Run 42	4.7	66.0	60.0	24.0			
Run 50	1.0	2.7	2.7	1.0	1.8	2.5	0.02

Table B7.1: Data from experiments at $n_0 = 0.43$

		Bed shear stress		v_e			
Test nr	**u_{flow}**	**Load cell**	**dp**	**lower limit**	**v_e**	**upper limit**	**c_{nb}**
	[m/s]	**[Pa]**	**[Pa]**	**[mm/s]**	**[mm/s]**	**[mm/s]**	**[-]**
Run 32	2.9	22.0	22.0	16.5			
Run 33	3.1	25.0	25.0		17.5	18.0	0.05
Run 34	4.0	46.0	44.0		29.5	32.0	0.06
Run 35	3.9	44.0	41.0	22.5	26.0		0.06
Run 36	2.1	12.0	12.0		8.0		0.03
Run 37	3.3	30.0	28.0			22.5	
Run 43	4.7	61.5	60.0			36.0	
Run 44	4.7	64.0	61.0		33.0		0.06
Run 45	4.5	61.0	58.0	27.0			

Table B7.2 Data from experiments at $n_0 = 0.47$

Appendix C. Porosity Bisschop

In the figure below one can see the experimental data of the present study and that of Bisschop (2018). The data of Bisschop (2018) has been separated into groups of different porosity. This figure shows that no trend can be found due to the porosity.

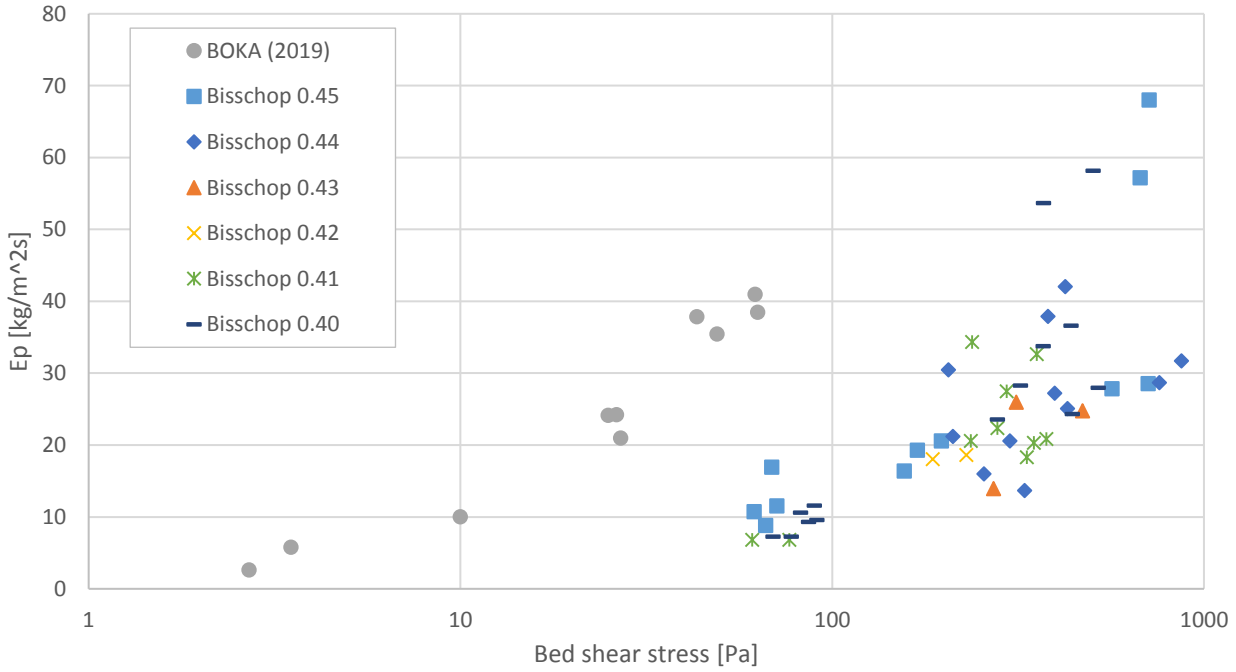

Figure C7.1: Pickup versus shear stress. Dataset of Bisschop (2018) is separated by porosity.

Appendix D. Iteration process Pugh & Wilson

Several iterations are necessary for this calculation. To be able to understand these iterations, the following equations are repeated here: Equation (2.40) Equation (2.16), Equation (2.17) and Equation (2.41):

$$dp_b = \frac{\tau_b \cdot w \cdot l}{A_b} = dp_w = \frac{\tau_w \cdot (2h + w) \cdot l}{A_w} \tag{D1}$$

$$\tau_b = \frac{\lambda}{8} \rho_w u^2 \tag{D2}$$

$$\frac{1}{\sqrt{\lambda}} = -2 \log\left(\frac{k_r}{3.7 D_h} + \frac{2.51}{Re \cdot \sqrt{\lambda}}\right) \tag{D3}$$

$$D_{h,w} = \frac{4A_w}{2h + w} \qquad D_{h,b} = \frac{4A_b}{w} \tag{D4}$$

The connections between the Equations is shown schematically in Figure D1. To avoid confusion, all symbols of the different bed shear stresses and differential pressures have been given in TABLE:

Symbol	Description
dp_b or dp_b	Differential pressure belonging to the bed associated area A_b
dp_w or dp_w	Differential pressure belonging to the wall associated area A_w
dp_mea or dp_{mea}	Measured differential pressure (belonging to the entire cross sectional area A)
$\tau_{dp,b}$	Bed shear stress calculated from differential pressure
τ_{lc}	Bed shear stress measured with the load cell
τ_{vp}	Bed shear stress calculated from the velocity profile

Table D1: Description of several symbols

As can be seen from Equation D1, dp_b and dp_w must be equal. This is the case at the intersections of the lines in Figure D2, which shows the calculated differential pressures for the bed and wall associated areas. In the figure one can also see the value of the measured differential pressure at u_{flow} = 2m/s (horizontal line). The intersections that are closest to this line are the most accurate. Lastly, the figure shows the corresponding $\tau_{dp,b}$ of some intersections. This value must agree with the bed shear stress measured by the load cell and the bed shear stress calculated with the velocity profile. Figure D1 shows the connection between the equations. The necessary iterations are indicated by the dashed boxes. Since the equation for the calculation of λ is implicit, iteration of Equation D3 itself is necessary. The values shown in both Figure D1 and D2 are all given for a flow velocity of 2 m/s which corresponds with the values of Figure 3.6 and Figure 3.7.

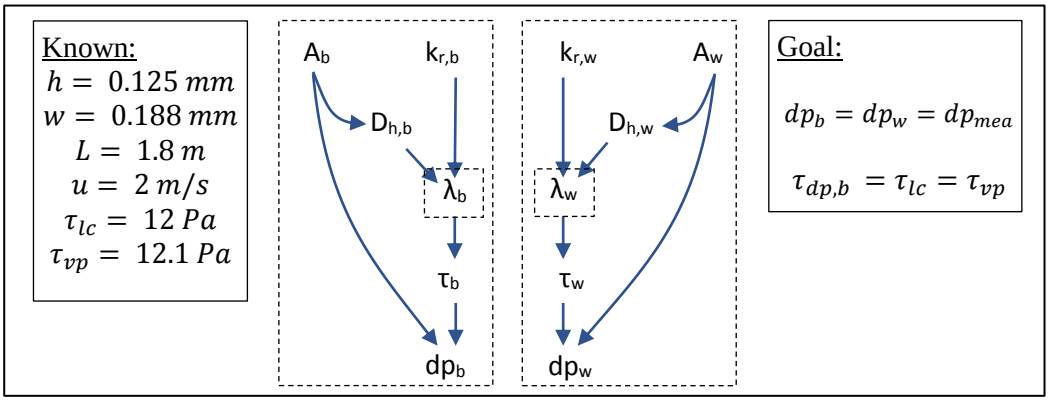

Figure D1: Schematic of the iteration process. The boxes with dashed lines show each iteration and the numbers indicate the order.

From Figure D2 it can be seen that the common wall roughness of 0.15 mm for galvanized steel will need to be combined with a bed roughness smaller than $1 \cdot d_{30}$ to match dp_{mea}. However, in addition to the fact that this is an unlikely bed roughness, in that situation, the calculated $\tau_{dp,b}$ is smaller than the measured τ_{lc}. Therefore it has been chosen to adjust the estimated wall roughness. When a combination of $k_{r,w} = 0.05$ and $k_{r,b} = 2 \cdot d_{90}$ are used, an intersection is found close to the dp_{mea} line. In addition to that the bed shear stresses all agree.

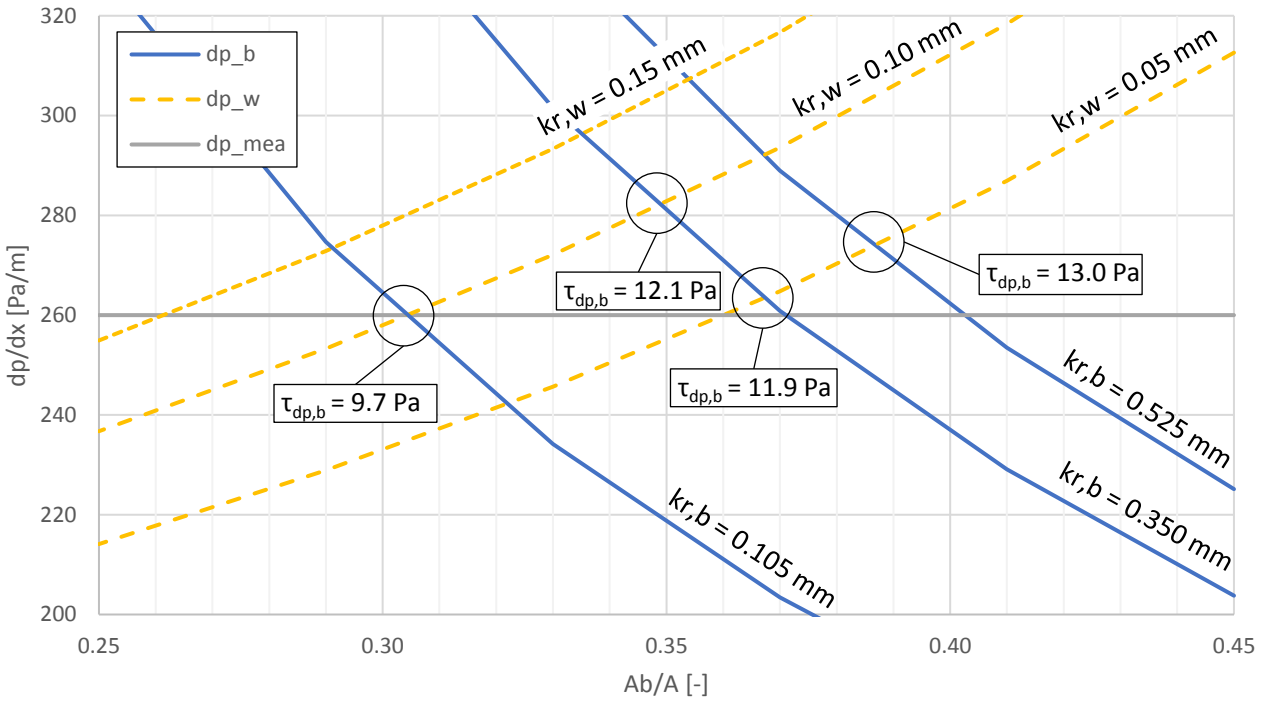

Figure D2: Calculated dp/dx as a function of the ratio A_b/A for u_{flow} = 2m/s. dp_mea is the measured pressure loss as seen in Figure 3.6.

Appendix E. Cheng (2016)

As mentioned in Chapter 4, the pickup function of Cheng (2016) is of interest to the present study since the experiments were performed in very similar experimental setups and the study is relatively recent. However, the experiments of Cheng (2016) were limited to flow velocities of 1 m/s ($\tau < 2$). In addition to that, Cheng (2016) mentions that his experiments cannot be well predicted by the function of Van Rijn (1984), even though Cheng (2016) based his experiments on the study of Van Rijn (1984).

When the pickup function of Cheng (2016) is compared to the data of the present study (Figure E1), it can be seen that the function largely underestimates the pickup. This is the case even though the function is based on very similar experiments to that of the present study. Clearly one or more processes that become dominant at higher velocities are missing from the pickup function of Cheng (2016). One again it is shown that it is risky to extrapolate the pickup functions to higher flow velocities.

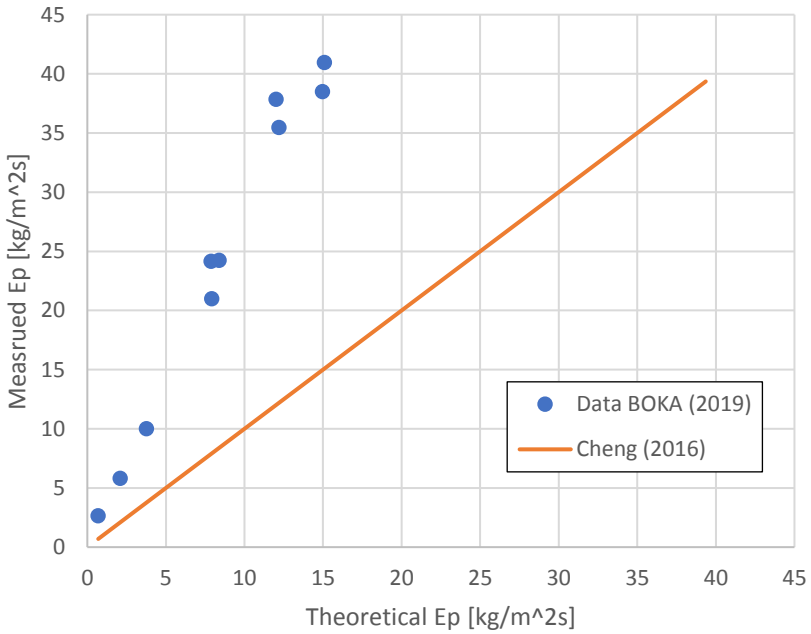

Figure E1: Comparison pickup function of Cheng (2016) and data BOKA (2019)

Appendix F. Photos

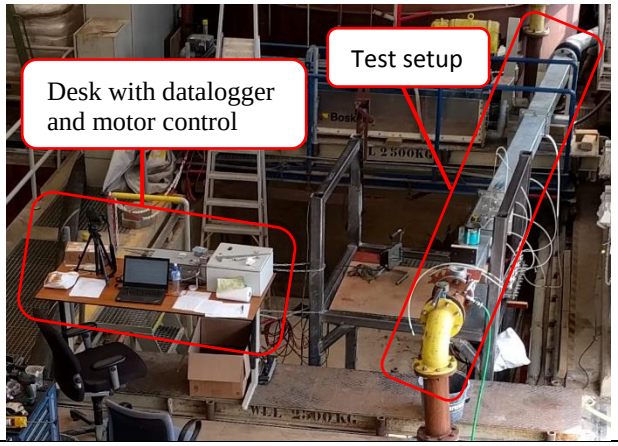

Figure F1: Overview of setup

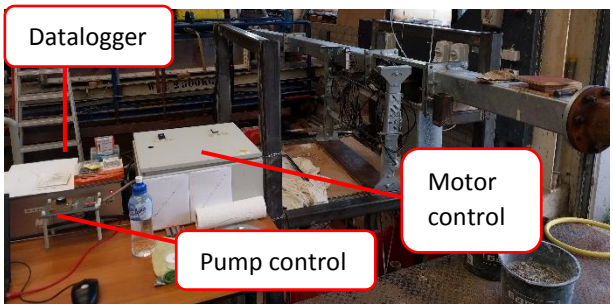

Figure F2: Overview of setup

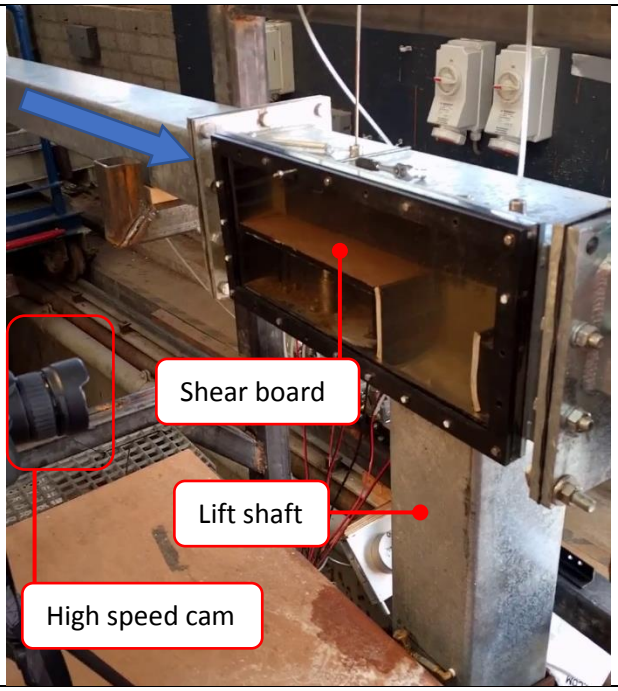

Figure F3: Front view of measuring section. The blue arrow shows the flow direction

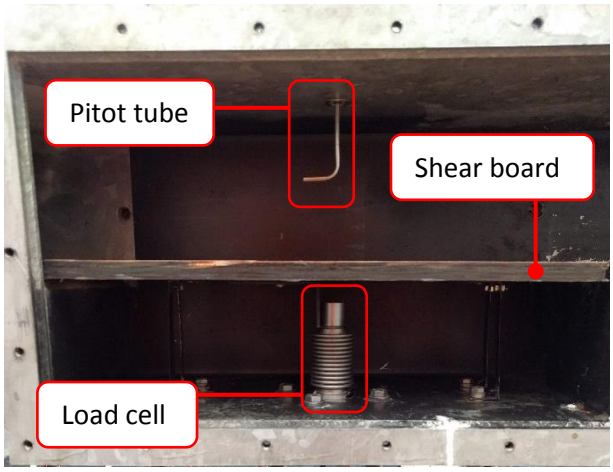

Figure F4: Load cell and Pitot tube

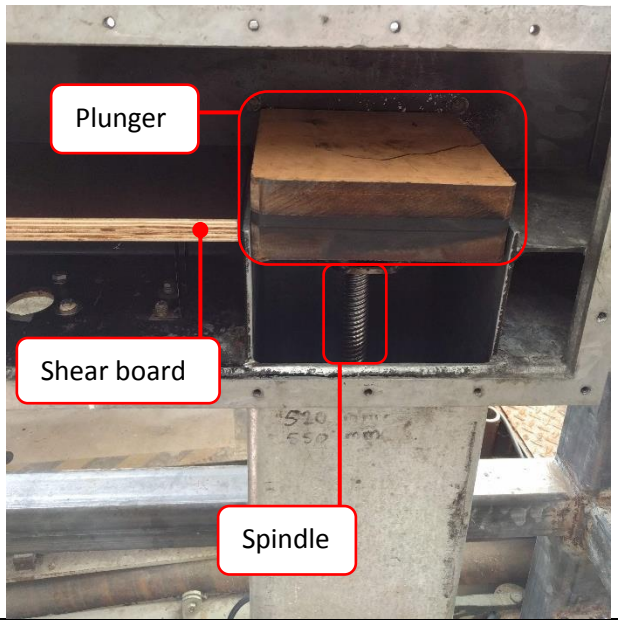

Figure F5: Lift plunger without seal

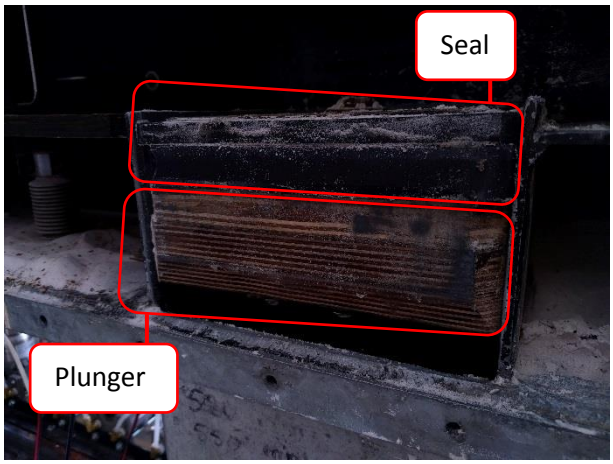

Figure F6: Lift plunger with seal

Figure F7: Inside of pipe. Fixed sand bed on bottom wall

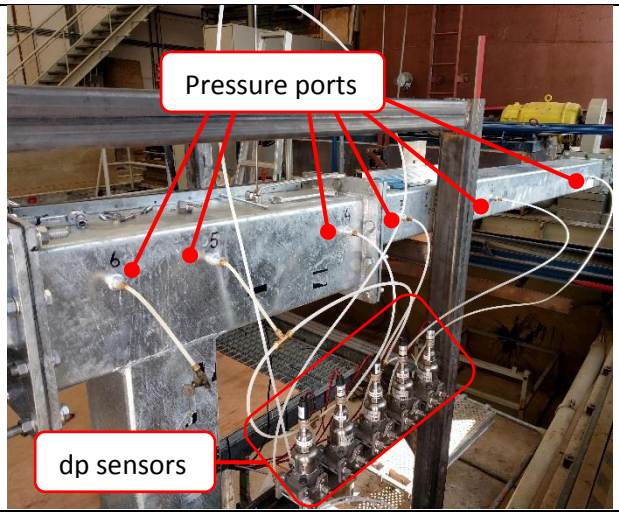

Figure F6: Rear view. Differential pressure sensors and connections. The configuration of the dp sensors in the photo is old

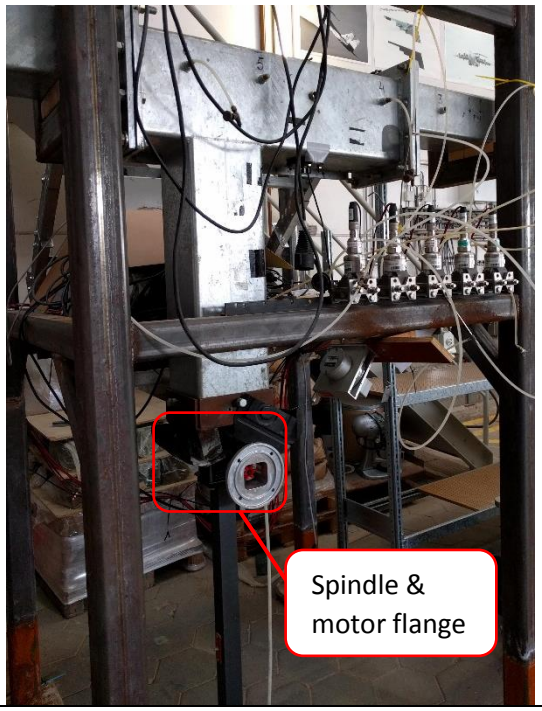

Figure F6: Rear view. Spindle and motor flange